


Laser-detected magnetic resonance induced by radio-frequency two-photon processes

Xu-xing Geng¹, Guoqing Yang², Pan-li Qi¹, Wangwang Tang¹, Shangqing Liang²,
Gao-xiang Li^{1,*} and Guang-ming Huang^{1,†}

¹*Department of Physics, Huazhong Normal University, Wuhan 430079, China*

²*College of Electronics and Information, Hangzhou Dianzi University, Hangzhou 310018, China*

 (Received 14 September 2020; revised 13 April 2021; accepted 28 April 2021; published 17 May 2021)

We have theoretically and experimentally investigated the laser-detected magnetic resonance induced by radio-frequency two-photon processes in $F_g = 4$ of D_1 line of cesium atoms. The effective Hamiltonian for the interaction between the two radio-frequency magnetic fields and sublevels at the ground state of $F_g = 4$ is derived. By appropriately selecting the frequencies of the two radio-frequency fields, the Raman two-photon process and the cascade two-photon process can occur, which induce the magnetic resonance detected through laser transmission spectra. The theoretical calculation results fit well with the experimental data. Our results maybe apply for measuring the high bandwidth radio-frequency magnetic fields in space and studying the magnetic-induction tomography.

DOI: [10.1103/PhysRevA.103.053112](https://doi.org/10.1103/PhysRevA.103.053112)

I. INTRODUCTION

With the development of natural science, the technology based on nonlinear optics theory has been developed rapidly. In the optical domain, technologies such as three-dimensional fluorescence imaging [1,2], optical data storage [3,4], two-photon excitation microscopy [5], and lithographic microfabrication [6] and some photopolymerization based on the multiphoton processes theory have been implemented. Numerous studies on the multiphoton processes are usually carried out in the interaction of light and nonlinear media, and direct excitation of the two-photon effect with a strong laser is a common method [7,8]. In the microwave domain, the numerous investigations of multiphoton processes is studied in the interaction of microwave electromagnetic fields and superconducting quantum circuits (SQCs), when microwave technology and cavity quantum electrodynamics (cavity QED) theory continue to deepen. Many extremely important applications, such as quantum manipulation [9,10], two-mode squeezing [11] and microwave degenerate parametric down-conversion [12], have been derived from the study of multiphoton processes of the microwave SQCs based on Josephson junctions. In the radio-frequency domain, nevertheless, the research on multiphoton processes in magnetic resonance transitions [13] is not particularly large, especially in studying the theory of atomic magnetic resonance in a weak offset field. In Ref. [14], Nettels *et al.* produced a multiphoton process in an experiment studying the magnetic resonance of cesium atoms trapped in a crystalline He matrix, and the atoms produced nonlinear Zeeman splitting effect in the static magnetic field used in the experiment. In their experiment, multiphoton transitions satisfying $\Delta m = N$ were observed, and applied the multiphoton transition effect to suppress systematic effects in the experiment of the search for permanent

electric-dipole moments (EDMs). However, in the case of magnetic resonance in a weak field whose Zeeman splitting ω_0 of the magnetic field is linear, there are not many studies on the multiphoton process induced by the radio-frequency magnetic field. Therefore, our research focuses on the multiphoton process in weak-field resonance. The difference from Nettels *et al.* [14] is that the offset magnetic field produces a linear Zeeman split, and the atoms are excited by two-photon process [15] to satisfy the $\Delta m = \pm 1$ transitions. We propose a method for measuring radio-frequency magnetic field using the laser-detected magnetic resonance induced by radio-frequency two-photon processes in which the linearly polarized laser field resonates with the transition from $F_g = 4$ to $F_e = 3$ of D_1 line of cesium atoms. The use of two orthogonal radio-frequency magnetic fields to interact with atoms is to excite the multiphoton process [16,17]. When the frequency ω_{RF} of the transverse radio-frequency field \mathbf{B}_{RF} and the frequency ω_m of the longitudinal radio-frequency field \mathbf{B}_m satisfy the condition $\omega_0 + \Delta\omega = \omega_m - \omega_{\text{RF}}$, the Raman two-photon process induces magnetic resonance. The shift $\Delta\omega$ is the AC Zeeman effect [18], which will be discussed in detail in the text. In the case of satisfying $\omega_0 + \Delta\omega = \omega_m + \omega_{\text{RF}}$, the cascade two-photon process induces magnetic resonance, as shown in Fig. 1. If the radio-frequency field \mathbf{B}_{RF} is turned off, the spectral lines disappear. In our experiment, if only a transverse radio-frequency field is used to excite the magnetic resonance system, the center frequency is the Larmor precession frequency ω_0 .

The precision measurement of the radio-frequency magnetic field is extremely important and valuable [19–25]. Nowadays, among the various devices for measuring radio-frequency magnetic fields, superconducting quantum interference device (SQUID) magnetometers [26,27], and atomic magnetometers based on magnetic resonance are of great interest and extensive research. Compared with the SQUID magnetometers, the atomic magnetometer has the advantages of not requiring low-temperature cooling, facilitating miniaturization and integration [28]. The alkali-metal atomic

*gaox@mail.ccnu.edu.cn

†gmhuang@mail.ccnu.edu.cn

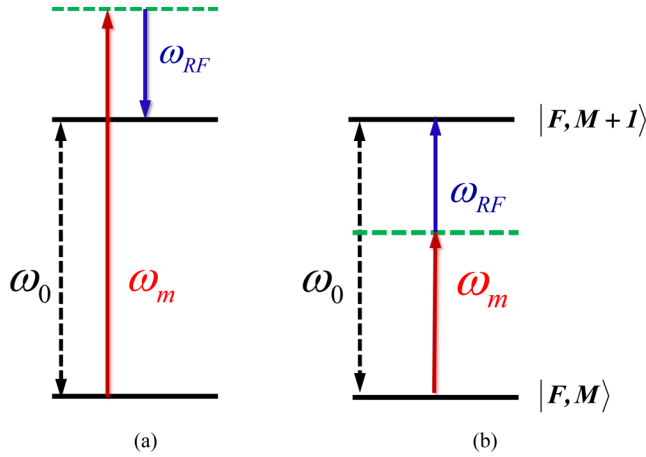


FIG. 1. (a) The Raman two-photon process. (b) The cascade two-photon process. Atomic sublevel with energy spacing ω_0 . The radio-frequency magnetic field \mathbf{B}_m with frequency ω_m and radio-frequency magnetic field \mathbf{B}_{RF} with frequency ω_{RF} act on the atomic transition $|F, M\rangle \leftrightarrow |F, M+1\rangle$.

magnetometer based on weak-field resonance generally used to measure a low-frequency magnetic field or a static magnetic field, and the sensitivity decreases as the frequency increases [29,30]. However, Savukov *et al.* [31] have used the improved circular-polarized light-pumped K-atom magnetometer to measure the radio-frequency magnetic field by tuning the Zeeman resonance of alkali-metal atoms to the rf frequency and partially suppressing spin-exchange collisions in the alkali-metal vapor. This is an amazing way to measure the radio-frequency magnetic field with an atomic magnetometer, but it is not easy to find the accurate Larmor frequency quickly in the process of changing the static magnetic field. In our model, the sublevel splitting generated by the offset magnetic field is kept constant, i.e., the Larmor precession frequency is unchanged, and the frequency of the known radio-frequency magnetic field is tuned. When the sum or difference of the frequency of the known radio-frequency magnetic field and the frequency of the unknown radio-frequency magnetic field matches the two-photon resonance condition, the measurement of the unknown radio frequency magnetic field can be realized. It will be more accurate and easier to measure the unknown radio-frequency magnetic field compared with tuning the offset field.

To clearly clarify the physical picture of the magnetic resonance excited by the radio-frequency two-photon process, we adopt a simpler pump-probe structure of linearly polarized light in this paper. The magnetic resonance excited by the two-photon process is the ground-state magnetic resonance of the sublevel and there is no direct relationship with the pump geometry of the optical pump. The pump geometry of the pump light mainly affects the polarization form of atoms. For example, low-power circularly polarized light pump induce orientation polarization and alignment polarization of atoms (under the condition of low optical power limit, it can be considered that there is only orientation polarization) [32], while low-power linearly polarized light pumps only cause atoms to produce alignment polarization [33]. The magnetic resonance signal is excited by the cascade two-photon process or Raman

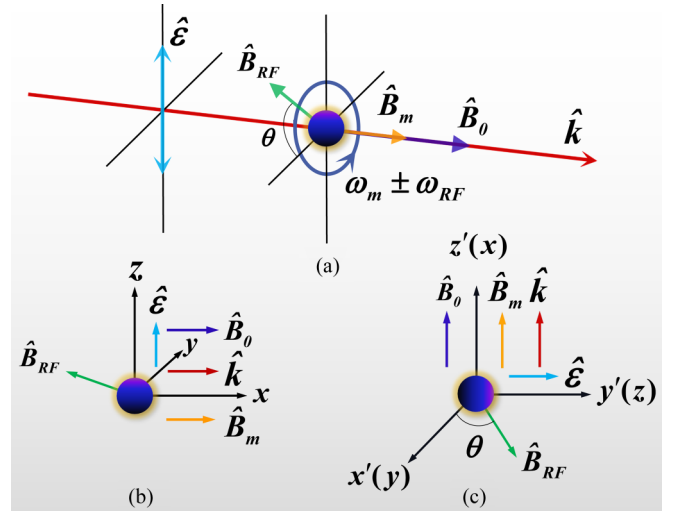


FIG. 2. (a) Parametrization of the theoretical model geometry, in which the radio frequency field \mathbf{B}_m and the offset field \mathbf{B}_0 are along the propagation direction of the linearly polarized light $\hat{\epsilon}$ and radio frequency field \mathbf{B}_{RF} on a plane perpendicular to the direction of light propagation. (b) The quantization axis set along the polarization direction of linearly polarized light. (c) The quantization axis set along the light propagation direction.

two-photon process generated by a transverse radio-frequency magnetic field \mathbf{B}_{RF} and a longitudinal radio-frequency magnetic field \mathbf{B}_m . We start (in Sec. II) from the establishment of the geometry and obtain the evolution equation of the atomic alignment of the magnetic resonance spectra through theoretical calculations. The theoretical analytical solutions of the magnetic resonance spectra are obtained. A detailed analysis by solving the steady-state solution of the evolution equations is performed. In Sec. III, we introduce the experimental setup and fit, analyze, and explain the magnetic resonance spectra excited by the cascaded two-photon process or Raman two-photon process, respectively. Finally, a summary for this paper is given in Sec. IV.

II. THEORY

A. Theoretical model and calculation

The atomic magnetic resonance in a weak field consists of three processes that are extremely important, which are polarization creation [34–38], atom-field interaction [39–42], and optical detection of magnetic resonance [43–46]. In our system model, as shown in Fig. 2(a), the linearly polarized light which resonances with the magnetic sublevels of the ground state $F_g = 4$ and the excited state $F_e = 3$ of the D_1 -line of alkali-metal cesium atoms causes alignment polarization of the atoms at the ground state. In the process of atom-field interaction, generally, magnetic resonance is excited by only a radio-frequency field [28,47]. When the frequency of the radio-frequency magnetic field matches the splitting of adjacent magnetic sublevels produced by the offset field, the magnetic resonance process occurs. The frequency of the radio-frequency magnetic field is the Larmor precession frequency $\omega_L = g_F \mu_B |B_0| = \gamma_F |B_0|$, where g_F , μ_B , and γ_F are the Landé factor, the Bohr magneton and the gyromagnetic

ratio, respectively. The difference between our system and traditional magnetic resonance is that the magnetic resonance is excited by the two-photon process instead of the single-photon excitation process. In our system, the offset field \mathbf{B}_0 causes the magnetic sublevels to produce linear Zeeman splitting. The Raman two-photon process or the cascade two-photon process is excited by the transverse radio-frequency magnetic field \mathbf{B}_{RF} and the longitudinal radio-frequency magnetic field \mathbf{B}_m , which are perpendicular to each other. The oscillating frequencies ω_{RF} and ω_m of the two radio-frequency magnetic fields are far from resonance with the sublevel splitting ω_0 . When the equivalent Larmor precession frequency produced by the two-photon process matches the splitting of two adjacent sublevels produced by the offset field \mathbf{B}_0 , the two-photon magnetic resonance is excited. In the optical detection process, the magnetic resonance induced by the magnetic-field affects the optical properties of the atoms. Generally, the information of the alignment-polarized atomic medium is obtained by measuring the transmission spectrum [48] and the Faraday rotation [49,50]. Meanwhile, the non-linear magneto-optical rotation approach considered in works such as Refs. [51] and [52] are also very interesting. Since our research focuses on the influence of the two-photon process on the profile and linewidth of the atomic absorption spectrum and the influence on the resonance position, we choose to detect the transmission absorption spectrum in this experiment. According to the above three processes, we use two-photon processes of two radio-frequency fields to excite weak-field resonance.

To calculate the magnetic resonance signal, physical quantities are put into the rotating frame $x'y'z'$ by rotating the coordinate axis. As shown in Fig. 2(c), the quantization axis is the direction of the offset field \mathbf{B}_0 . It is assumed that the frequency of the atomic magnetic moment precession is much larger than the relaxation coefficient of the atomic magnetic moment. In this frame, $\mathbf{B}_{z'} = (B_0 + B_m \cos \omega_m t) \mathbf{e}_{z'}$, $\mathbf{B}_{x'} = B_{\text{RF}} \cos \theta \cos \omega_{\text{RF}} t \mathbf{e}_{x'}$ and $\mathbf{B}_{y'} = B_{\text{RF}} \sin \theta \cos \omega_{\text{RF}} t \mathbf{e}_{y'}$. According to $\mathbf{H}_B = -\boldsymbol{\mu} \cdot \mathbf{B}_{\text{tot}} = g_F \mu_B (F_{-1} B^{-1} + F_0 B^0 + F_1 B^1)$ and $B^\pm = \mp \sqrt{\frac{1}{2}} (B_{x'} \mp i B_{y'})$, $B^0 = B_{z'}$, where F_i is the angular-momentum component in the covariant spherical basis representation and B^j is the magnetic field component in the contravariant spherical basis representation, the Hamiltonian of the interaction of the magnetic field with the ground state atomic system is specifically denoted

$$\begin{aligned} \mathbf{H}_{B_{\text{tot}}} = & \omega_0 F_0 + \Omega_m F_0 \cos \omega_m t \\ & + \frac{1}{\sqrt{2}} \Omega_{\text{RF}} F_{-1} e^{i\theta} \cos \omega_{\text{RF}} t \\ & - \frac{1}{\sqrt{2}} \Omega_{\text{RF}} F_1 e^{-i\theta} \cos \omega_{\text{RF}} t, \end{aligned} \quad (1)$$

where $\omega_0 = g_F \mu_B B_0$, $\Omega_m = g_F \mu_B B_m$, and $\Omega_{\text{RF}} = g_F \mu_B B_{\text{RF}}$. Considering the conditions $\omega_m, |\omega_0 - \omega_{\text{RF}}| \gg \Omega_{\text{RF}}$ and ensuring that the frequency of the two radio-frequency fields are highly detuned from the frequency difference between two adjacent magnetic sublevels, we derive the effective Hamiltonian of $\mathbf{H}_{B_{\text{tot}}}$. According to James' effective Hamiltonian theory [53,54] $\mathbf{H}_{\text{eff}} = -iH(t) \int^t dt' H(t')$, the effective Hamiltonian

of $\mathbf{H}_{B_{\text{tot}}}$ is

$$\begin{aligned} \mathbf{H}_{B_{\text{tot}}}^{\text{eff}} \approx & \Delta \omega F_0 - \frac{1}{\sqrt{2}} \Omega e^{i\theta} F_{-1} e^{i(\omega_m + \omega_{\text{RF}} - \omega_0)t} \\ & + \frac{1}{\sqrt{2}} \Omega e^{-i\theta} F_1 e^{-i(\omega_m + \omega_{\text{RF}} - \omega_0)t} \\ & - \frac{1}{\sqrt{2}} \Omega e^{i\theta} F_{-1} e^{i(\omega_m - \omega_{\text{RF}} - \omega_0)t} \\ & + \frac{1}{\sqrt{2}} \Omega e^{-i\theta} F_1 e^{-i(\omega_m - \omega_{\text{RF}} - \omega_0)t}. \end{aligned} \quad (2)$$

The detailed derivation of Eq. (2) is given in Appendix A. Assuming $(\omega_m \pm \omega_{\text{RF}}) - \omega_0 = \delta_j$, ($j = S, D$), where indicator D indicates the difference-frequency process and indicator S indicates the sum-frequency process, the effective Hamiltonian of the sum(or difference)-frequency process is

$$\mathbf{H}_j^{\text{eff}} = \Delta \omega F_0 - \frac{1}{\sqrt{2}} \Omega e^{i\theta} F_{-1} e^{i\delta_j t} + \frac{1}{\sqrt{2}} \Omega e^{-i\theta} F_1 e^{-i\delta_j t}, \quad (3)$$

where

$$\Delta \omega = \frac{\Omega_{\text{RF}}^2}{8} \left(\frac{1}{\omega_0 - \omega_{\text{RF}}} + \frac{1}{\omega_0 + \omega_{\text{RF}}} \right) \quad (4)$$

is to make slight shifts of the frequency of the magnetic sublevels, and

$$\Omega = \frac{\Omega_{\text{RF}} \Omega_m}{4\omega_m} \quad (5)$$

is the Rabi frequency of the equivalent radio-frequency magnetic fields. According to the effective Hamiltonian (3), we can find that the first term of the effective Hamiltonian is $\Delta \omega$, which being the sublevel shift produced by the radio-frequency magnetic field called the AC Zeeman shift [18]. The AC Zeeman shift $\Delta \omega$ is only determined by the horizontal radio-frequency field \mathbf{B}_{RF} and ω_0 , and is independent of the radio-frequency field \mathbf{B}_m in the z direction, because the two equivalent magnetic sublevel shifts generated by \mathbf{B}_m are equal in magnitude and opposite to each other, resulting in mutual cancellation. Therefore, the equivalent Larmor frequency of the system is $(\omega_0 + \Delta \omega)$. Only when condition $\omega_0 + \Delta \omega = \omega_m - \omega_{\text{RF}}$ or $\omega_0 + \Delta \omega = \omega_m + \omega_{\text{RF}}$ is present can an atom absorb or emit two radio-frequency photons to produce a two-photon process. As shown in Fig. 1, under condition $\omega_0 + \Delta \omega = \omega_m - \omega_{\text{RF}}$, the atom will absorb a π radio-frequency photon, and then release a σ radio-frequency photon to form a Raman two-photon process. In the case of condition $\omega_0 + \Delta \omega = \omega_m + \omega_{\text{RF}}$, the atom will simultaneously absorb a π radio-frequency photon and a σ radio-frequency photon to form a cascade two-photon process. It is worth noting that although the atom absorbs two photons, it satisfies the $\Delta m = \pm 1$ transition. The atomic transition strength Ω is proportional to the ratio of the product of the Rabi frequencies of two radio-frequency magnetic fields and inversely proportional to ω_m .

The effective Hamiltonian of the Raman two-photon process and the cascade two-photon process in the rotating frame is

$$\tilde{\mathbf{H}}_j^{\text{eff}} = \Delta_j F_0 - \frac{1}{\sqrt{2}} \Omega e^{i\theta} F_{-1} + \frac{1}{\sqrt{2}} \Omega e^{-i\theta} F_1, \quad (6)$$

where $\Delta_j = \Delta\omega - \delta_j$. From Eq. (6), we find that the form of the effective Hamiltonian is the same as that of the traditional magnetic resonance based on atomic alignment [43]. The master equation for the evolution of the density matrix of the system is

$$\frac{d}{dt}\rho = -\frac{i}{\hbar}[\tilde{H}_j^{\text{eff}}, \rho] + \mathcal{L}\rho, \quad (7)$$

where $\mathcal{L}\rho$ represents the relaxation process of the system. The density-matrix element ρ is expanded into a form $\rho = \sum_{k=0}^F \sum_{q=-k}^k m(F'F)_{k,q} T(F'F)_{k,q}$ of atomic multipole moments through a set of complete irreducible tensor bases [55–57], and then brought into the master equation to obtain a matrix equation of atomic second-order multipole moment evolution with time

$$\frac{dm_{2,q}}{dt} = \sum_{q'} H_{qq'}^{(2)} m_{2,q'} + \mathcal{L}m_{2,q}, \quad q = -2, -1, 0, 1, 2. \quad (8)$$

Here $H_{qq'}^{(2)}$ is the Hamiltonian of the system in the atomic multipole moment bases, and the specific form of the $H_{qq'}^{(2)}$ matrix is

$$H_{qq'}^{(2)} = \begin{pmatrix} -2i\Delta_j & i\tilde{\Omega}^* & 0 & 0 & 0 \\ i\tilde{\Omega} & -i\Delta_j & i\sqrt{\frac{3}{2}}\tilde{\Omega}^* & 0 & 0 \\ 0 & i\sqrt{\frac{3}{2}}\tilde{\Omega} & 0 & i\sqrt{\frac{3}{2}}\tilde{\Omega}^* & 0 \\ 0 & 0 & i\sqrt{\frac{3}{2}}\tilde{\Omega} & i\Delta_j & i\tilde{\Omega}^* \\ 0 & 0 & 0 & i\tilde{\Omega} & 2i\Delta_j \end{pmatrix}, \quad (9)$$

where $\tilde{\Omega} = \Omega e^{i\theta}$ and $\tilde{\Omega}^* = \Omega e^{-i\theta}$. The second term $\mathcal{L}m_{2,q}$ represents the evolution of the relaxation of atomic multipole moments. The atomic magnetic moment relaxation process $\mathcal{L}m_{2,q}$ is mainly composed of three types of relaxation processes: the optical pump relaxation process $\mathcal{L}_L\rho$, the ground-state spin-exchange collision relaxation process $\mathcal{L}_{se}\rho$, and the transit relaxation process $\mathcal{L}_{\text{transit}}\rho$. A detailed derivation is given in Appendix B. In the $x'y'z'$ frame, its specific form can be expressed as

$$\mathcal{L}m_{2,q} = \begin{pmatrix} -\Gamma_{22}m_{2,2} \\ -\Gamma_{21}m_{2,1} \\ -\Gamma_{20}m_{2,0} + \Gamma_{00}m_{0,0} \\ -\Gamma_{21}m_{2,-1} \\ -\Gamma_{22}m_{2,-2} \end{pmatrix}, \quad (10)$$

where $\Gamma_{20} = \gamma + \frac{31}{64}\gamma_{se} + \frac{271}{1134}\Gamma_L$, $\Gamma_{21} = \gamma + \frac{31}{64}\gamma_{se} + \frac{323}{1512}\Gamma_L$, $\Gamma_{22} = \gamma + \frac{31}{64}\gamma_{se} + \frac{26}{189}\Gamma_L$, and $\Gamma_{00} = -\frac{7}{324}\sqrt{77}\Gamma_L$. The coefficient Γ_{20} is the longitudinal alignment relaxation rate, coefficients Γ_{21} and Γ_{22} are the transverse alignment relaxation rates, and coefficient Γ_{00} is the monopole moment relaxation rate. Γ_{2q} ($q = 0, 1, 2$) is composed of the optical pump relaxation rate Γ_L [57], the ground-state spin-exchange collision relaxation rate γ_{se} [39], and the transit relaxation rate γ [58]. The monopole moment $m_{0,0}$ is related to the total population of ground-state atoms, which is used as an injection of the alignment. According to Appendix C, we find that the polarization of the atomic ensemble is related to the relaxation processes and rf excitation. Among the relaxation processes that affect the polarization of atoms, the

influence of the optical pump on the ensemble is dominant, i.e., alignment polarization is produced.

We assume that the pump light intensity is weak enough ($|\Omega_0| \ll \Gamma$). In the frame $x'y'z'$, the absorption coefficient [40,43,58,59] is

$$\alpha = \frac{\alpha_0}{9} \left(14m_{0,0} + \frac{\sqrt{77}}{2}m_{2,0} \right), \quad (11)$$

where the coefficient $\alpha_0 = 4\pi\omega_0 N/\hbar c$ is just a constant. The detailed derivation is in Appendix B. The change of alignment $m_{2,0}$ is related to the variation of the Rabi frequencies Ω_m and Ω_{RF} , the oscillation frequencies ω_m and ω_{RF} , and the detuning Δ_j . Therefore, the component of the absorption coefficient α of the pump-probe light mainly depends on alignment $m_{2,0}$. The laser transmission spectrum is usually used in the experiments to analyze the evolution of the atomic multipole moment. For the convenience of description, the laser transmission spectrum signal is defined as

$$P_j(\Delta_j, \Omega_m, \Omega_{\text{RF}}, \omega_m, \omega_{\text{RF}}) = C_0 m_{2,0}, \quad (12)$$

where C_0 is a constant associated with the optical power and amplifier gain factors [48,60].

B. Results and theoretical analysis

The magnetic resonance DC signal of Raman two-photon process or cascade two-photon process of laser transmission spectrum is

$$P_j^{dc} = C_0 m_{0,0} \frac{\Gamma_{00}}{\Gamma_{20}} \left\{ 1 - \frac{3\Gamma_{21}\Omega^2}{(\Delta_j^2 + x_1)\Gamma_{20}} + \frac{3[4x_2\Gamma_{21} + \Gamma_{22}(\Gamma_{21}\Gamma_{22} + \Omega^2)]\Omega^2}{4(\Delta_j^2 + x_1)(\Delta_j^2 + x_2)\Gamma_{20}} \right\}, \quad (13)$$

with

$$x_1 = \Gamma_{21}^2 + \left(\frac{3\Gamma_{21}}{\Gamma_{20}} + \frac{2\Gamma_{21}}{\Gamma_{22} - 2\Gamma_{21}} \right) \Omega^2 + \frac{3[\Gamma_{20}(2\Gamma_{21} + \Gamma_{22}) - 3\Gamma_{21}^2]}{\Gamma_{20}^2(\Gamma_{22}^2 - 4\Gamma_{21}^2)} \Omega^4 \quad (14)$$

and

$$x_2 = \frac{\Gamma_{22}^2}{4} - \frac{\Gamma_{22}}{\Gamma_{22} - 2\Gamma_{21}} \Omega^2 - \frac{3[\Gamma_{20}(2\Gamma_{21} + \Gamma_{22}) - 3\Gamma_{21}^2]}{\Gamma_{20}^2(\Gamma_{22}^2 - 4\Gamma_{21}^2)} \Omega^4. \quad (15)$$

In the case of satisfying $\Gamma_{20} \approx \Gamma_{22} \approx \Gamma_{21}$ [43] and $\Omega \ll \Gamma_{21}$, the transmission spectrum P_j^{dc} is further reduced to

$$P_j^{dc} \approx C_0 \frac{\Gamma_{00}}{\Gamma_{21}} \left(\frac{1}{3} - \frac{\Omega^2}{\Delta_j^2 + \Gamma_{21}^2} \right). \quad (16)$$

According to Eq. (13), the transmission spectrum signal P_j^{dc} of the magnetic resonance generated by the two-photon excitation is composed of three terms. The first term is that the constant term has no effect on the information carried by the transmission spectrum. It simply means that the interaction of the laser with the atom causes the atomic system to

establish a new dynamic equilibrium to reach a steady state, i.e., the atom is repolarized. Considering the fitting between experiment and theory, all fitting curves ignore this item. The second term is the linear absorption term, which is the quasi-Lorentz absorption line type. The process for sum-frequency excited magnetic resonance can be interpreted as a cascade two-photon absorption process [61]. The process of magnetic resonance for difference-frequency excitation can be interpreted as a Raman two-photon process [62]. The linewidth and height of the absorption peak become larger as Ω increases. In the limiting case of low rf and optical field strength, the transmission spectrum P_j^{dc} can be simplified to Eq. (16). The amplitude of the transmission spectrum is not only related to the Rabi frequency Ω but also related to the ratio of the relaxation coefficients of the monopole moment and the alignment of the atoms. The second term of Eq. (16) is the standard Lorentz line type with linewidth Γ_{21} . The linewidth Γ_{21} is also the linewidth limit of this system. According to Eq. (13), the conditions for achieving a narrow linewidth transmission spectrum are sufficient low rf power and optical power. However, sufficiently low rf power and optical power will result in extremely small signal amplitudes. From an experimental point of view, narrowing the linewidth comes at the expense of the signal-to-noise ratio. The third term of P_j^{dc} in Eq. (13) is the higher-order effect of the alignment, which can be understood as a modification of the second term, which is a type of multiplication of two Lorentz functions.

Figure 3(a) shows the magnetic resonance transmission spectra excited by Raman two-photon processes without changing ω_0 , Ω_{RF} , and Ω_m . As the frequencies of the two radio frequency fields increase, the peaks of the spectral lines decrease monotonically. This phenomenon can be explained by Eq. (5). The equivalent Rabi frequency Ω is inversely proportional to the frequency ω_m of the longitudinal radio frequency field. A smaller equivalent Rabi frequency results in a weaker coupling between the field and the atom, so the peak value is reduced. The same phenomenon can be seen in the magnetic resonance spectrum excited by the cascade two-photon process in Fig. 3(b). Figure 4(a) shows the theoretically calculated magnetic resonance transmission spectra excited by Raman two-photon processes. The frequency ω_m of the longitudinal radio frequency field B_m and the frequency ω_{RF} of the transverse radio frequency field B_{RF} do not strictly match the split frequency ω_0 of the offset field B_0 . This is caused by the AC Zeeman shift. Similarly, there is still an energy-level shift in the magnetic resonance excited by the cascade two-photon process in Fig. 4(b). We verify the theoretical model through experiments in subsequent work.

III. EXPERIMENT

A. Experimental setup

The experimental setup is illustrated in Fig. 5. To detect the magnetic resonance signals generated by the two-photon processes, we placed a cesium atomic cell with a diameter of 25 mm and a length of 30 mm in a large solenoid in the magnetic shielding cylinder. To reduce the linewidth of the atom to the order of ten hertz, we have coated a layer of paraffin on the inner wall of the gas cell to reduce the dissipation caused by the collision of the atom with the wall of the cell. The

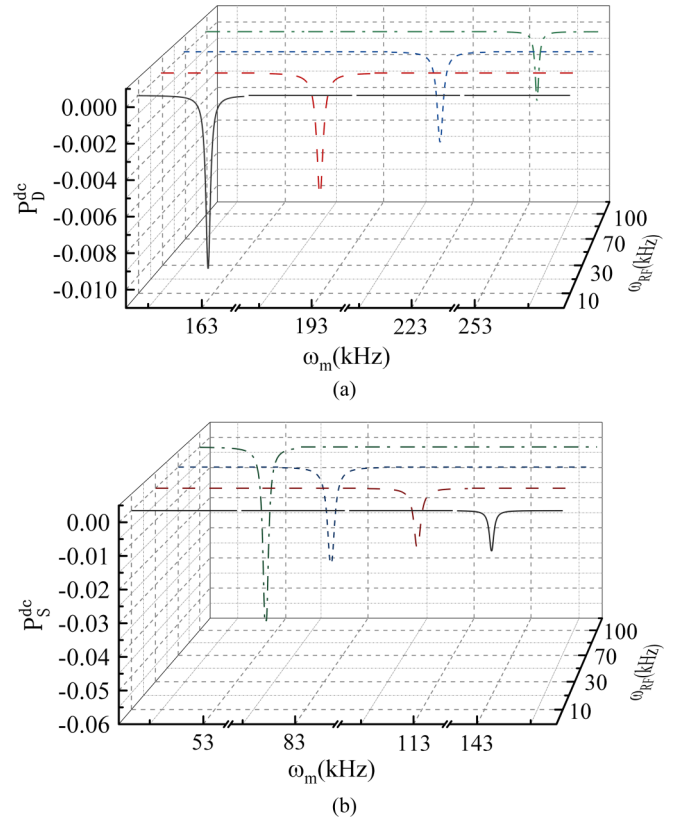


FIG. 3. The theoretically calculated transmission spectra signal P_j^{dc} of magnetic resonance without changing ω_0 , Ω_{RF} , and Ω_m . (a) The magnetic resonance excited by the Raman two-photon process. (b) The magnetic resonance excited by the cascade two-photon process.

offset magnetic field \mathbf{B}_0 is generated by a large solenoid driven by a precision current source (Keysight B2912A), which is a uniform magnetic field in the range of 0 to 5×10^4 nT. The magnetic shielding cylinder is composed of a four-layer μ -metal cylinder. In the central region of the magnetic shielding cylinder, even if the magnetic field reaches 5×10^4 nT, the fluctuation of the magnetic field is less than 2 nT, whose fluctuation is composed of the noise of the precision current source and the inhomogeneity of the residual magnetism in space. We use a Toptica DL pro laser as the light source with a spot diameter of 2.5 mm. The Toptica DigiLock 110 was used to lock the laser to the $F_g = 4 \rightarrow F_e = 3$ transition of the D_1 line of the alkali-metal cesium atom. The power of the laser can be tuned using a half-wave plate and PBS. To ensure the polarization purity of linearly polarized light, a Glan Taylor linear polarizer is placed in front of the magnetic shielding cylinder. The two radio-frequency fields \mathbf{B}_{RF} and \mathbf{B}_m , which are perpendicular to each other, are generated using Helmholtz coils with a diameter of 100 mm. The two perpendicular coils are respectively driven by two different arbitrary waveform generators. When the frequency of the Raman two-photon process (or cascade two-photon process) generated by two orthogonal radio-frequency magnetic fields matches the magnetic resonance conditions, the resonance signal can be detected by the probe light. The transmitted laser signal is received by a photodetector (Newport optical receiver

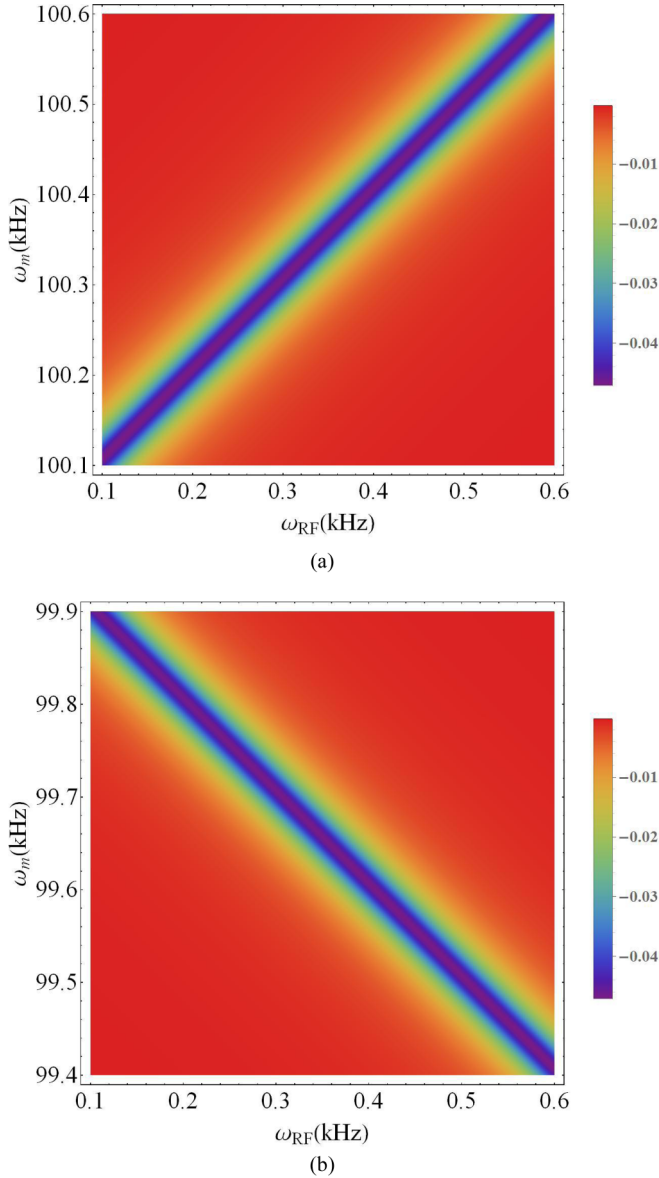


FIG. 4. The theoretically calculated transmission spectra signal P_j^{dc} of magnetic resonance with the parameter $\omega_0 = 100$ kHz. (a) The magnetic resonance excited by the Raman two-photon process. (b) The magnetic resonance excited by the cascade two-photon process.

2031) and converted into electrical signals for transmission to a digital oscilloscope (Tektronix TDS2014C). Next, we show and analyze the transmission spectra displayed by a digital oscilloscope.

B. Fitting and analysis of magnetic resonance spectra excited by Raman two-photon process

Analytical solution of the magnetic resonance excited by two-photon process is valid under the conditions of weak laser power and weak equivalent Rabi frequency Ω . Weak pump-probe laser conditions ensure that we consider the rationality of atomic monopole moment and atomic alignment without considering other high-order atomic polarization moments such as hexadecapole moment and hexacontatetrapole

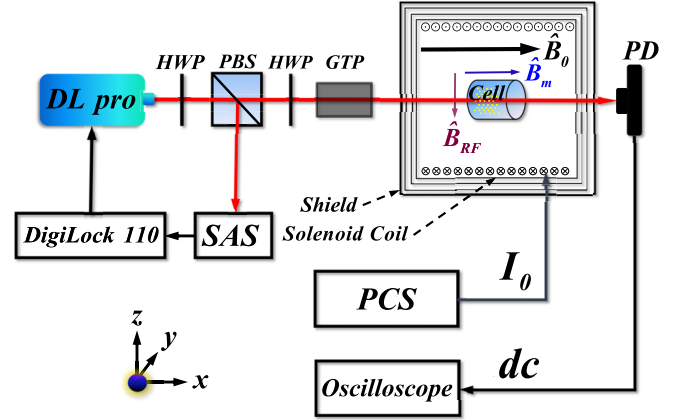


FIG. 5. Schematic of the experimental setup: tunable diode laser with digital control (DL pro), digital laser locking module (DigiLock 110), saturated absorption spectroscopy (SAS), half-wave plate (HWP), polarizing beam splitter (PBS), Glan-Taylor linear polarizer (GTP), cesium atomic cell, Helmholtz coils (not shown in the picture), low-noise solenoid coil, four-layer alloy cylinder shield, photodetector (PD), arbitrary waveform generators (AWG, not shown in the picture), precision current source (PCS), and oscilloscope. The coordinate frame shown in the figure is consistent with the laboratory frame in the theoretical model. Details of all installations can be found in the text.

moment. As shown in Fig. 6(a), the results predicted by the theoretical model are well verified by the experimental data fitting. The magnetic resonance curve is measured at the center frequency by scanning longitudinal rf fields \mathbf{B}_m is about 172.428 kHz. The experimental data are fit with the same physical parameters. The relaxation rate is mainly composed of the optical pump relaxation process $\mathcal{L}_L\rho$, the spin-exchange collision relaxation process $\mathcal{L}_{se}\rho$ in the ground state $F_g = 4$, and the transit relaxation process $\mathcal{L}_{\text{transit}}\rho$. The frequency ω_{RF} of the transverse radio-frequency magnetic field \mathbf{B}_{RF} is 20 kHz, and the frequency ω_m of the longitudinal radio-frequency magnetic field \mathbf{B}_m is 172.428 kHz. If the radio-frequency field \mathbf{B}_{RF} is turned off, the spectral lines disappear. In our experiment, if only a transverse radio-frequency field is used to excite the magnetic resonance system, the center frequency is the Larmor precession frequency $\omega_0 = 152.426$ kHz. The equivalent Larmor precession frequency produced by Raman two-photon process is about 152.428 kHz. We find that the magnetic resonance signal excited by Raman two-photon process is different from the magnetic resonance signal excited by a transverse radio-frequency field. The former will produce a frequency shift $\Delta\omega$ (which is about 2 Hz), but the latter will not. Equation (13) shows that the position of the resonance peak is at $\Delta_D = 0$. The detuning Δ_D contains the Zeeman shift item $\Delta\omega$. Only when the Raman process is satisfied, $\omega_0 + \Delta_D = \omega_m - \omega_{\text{RF}}$, will the system resonate. For a traditional magnetic resonance process excited by a transverse radio-frequency magnetic field, as long as the frequency of the radio-frequency field is equal to the Larmor precession frequency, the system will resonate. In Fig. 6(b), the frequency of the transverse radio-frequency magnetic field \mathbf{B}_{RF} is set to 172.426 kHz, and the

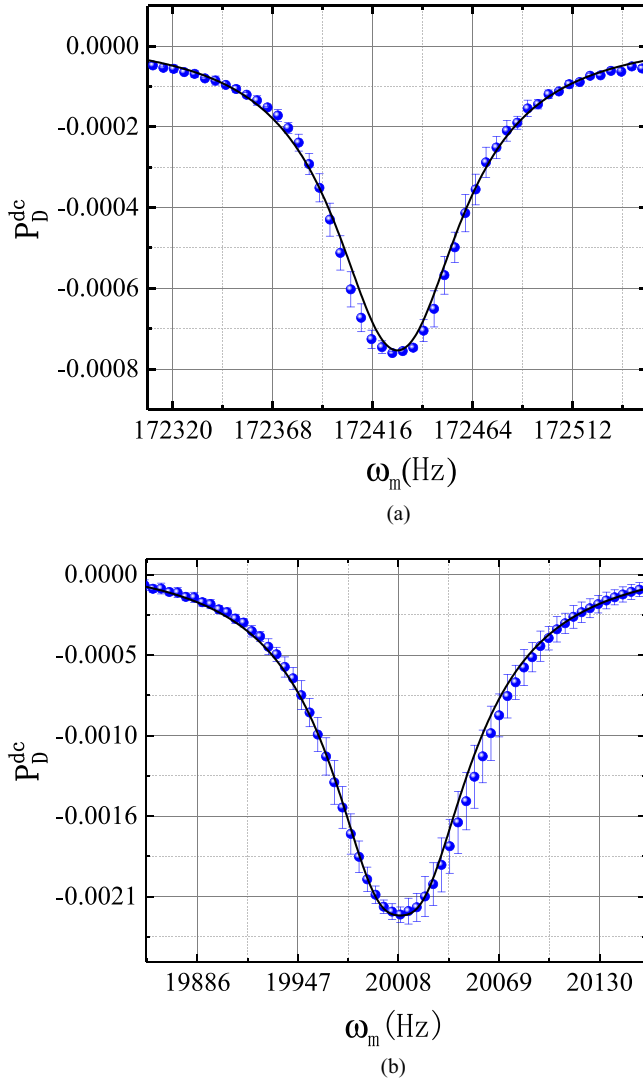


FIG. 6. Resonance spectra of Raman two-photon process, which are plotted as fractional transmission of the pump beam. The solid line (black) is the lineshape of the theoretical analytical solution fitting given by Eqs. (13) with three differently independent relaxation coefficients $\gamma \approx 20$ Hz, $\gamma_{se} \approx 20$ Hz, and $\Gamma_L \approx 33$ Hz. The Rabi frequency Ω_{RF} of the transverse radio-frequency magnetic field is about 1.2 kHz. The blue solid dots with error bars represent the measured experimental data. The optical power is about $10 \mu W$. (a) The frequency ω_m of longitudinal radio-frequency magnetic field is about 172.428 kHz. The frequency ω_{RF} of the transverse radio-frequency magnetic field is 20 kHz. (b) The frequency ω_m of longitudinal radio-frequency magnetic field is about 20.008 kHz. The frequency ω_{RF} of the transverse radio-frequency magnetic field is 172.426 kHz.

frequency of the longitudinal radio frequency magnetic field \mathbf{B}_m is about 20.008 kHz. The AC Zeeman shift $\Delta\omega$ caused by the transverse radio-frequency magnetic field is about -8 Hz. This phenomenon can be explained by Eq. (4). It determines the shift of the system energy level, and the magnitude of $\Delta\omega$ is restricted by the Rabi frequency Ω_{RF} and oscillation frequency ω_{RF} of the transverse radio-frequency field \mathbf{B}_{RF} . The energy-level shift calculated according to the definition of AC Zeeman shift $\Delta\omega$ is 2.4 and -8.4 Hz, respectively.

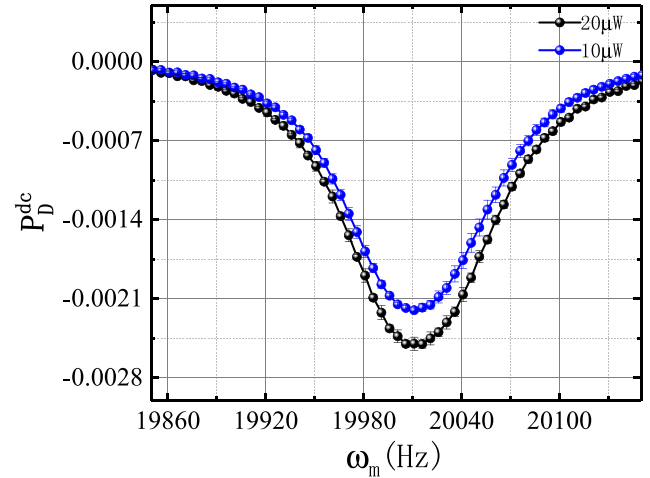


FIG. 7. The magnetic resonance transmission spectra of Raman two-photon process, which is plotted as fractional transmission of the pump beam. The frequency ω_m of longitudinal radio-frequency magnetic field is about 20.007 kHz. The frequency ω_{RF} of the transverse radio-frequency magnetic field is 172.426 kHz. The optical powers of blue and black solid dots with error bars are $10 \mu W$, respectively.

The theoretical calculation is basically consistent with the experimental measurement. This phenomenon of energy-level shift can reflect the physical characteristics of the amplitude and frequency of the transverse radio-frequency field \mathbf{B}_{RF} .

Figure 7 shows the magnetic resonance spectra excited by different optical powers. The peak value and linewidth of the transmission spectrum increase as the optical power increases. Since the absorption of photons by atoms is proportional to the Rabi frequency of the coupling of light and atoms, the peak of the transmission spectrum increases with the increase of optical power. The reason for the increase in linewidth is due to the phenomenon of optical power broadening. According to the linewidth formula (14), in the case of weak Rabi frequency Ω , the linewidth is mainly decided by the contribution of the first term Γ_{21} . The transverse alignment relaxation rate Γ_{21} is mainly composed of the optical pump relaxation rate and the atomic spin-exchange collision relaxation rate in the ground state. When the optical power gradually increases, the relaxation rate of the optical pump also increases. Therefore, the linewidth will increase as the optical power increases. It can be found from Fig. 8 that the peak of the transmission spectra of magnetic resonance increases with the increase of the equivalent Rabi frequency Ω generated by the Raman two-photon process. In the experiment, we change the Rabi frequency Ω of the Raman two-photon process by changing the Rabi frequency Ω_{RF} of the transverse radio frequency magnetic field. Considering the case of small Ω , Eq. (13) shows that the peak of the transmission spectrum is proportional to the square of the Rabi frequency Ω . As shown in Fig. 9, in the case of low optical power and small Rabi frequency Ω , the linewidth of magnetic resonance increases monotonically with the continuous increase of Ω . This phenomenon can be explained by Eq. (14). When the equivalent Rabi frequency Ω produced by the Raman two-photon is very

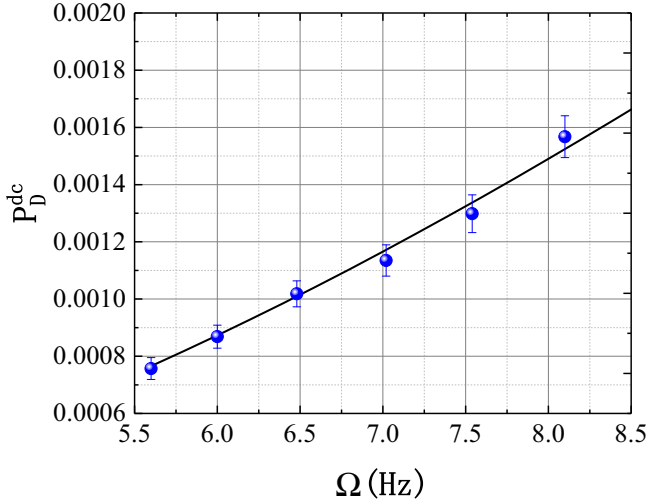


FIG. 8. The amplitudes of the magnetic resonance transmission spectra of Raman two-photon process for different Ω , which is plotted as fractional transmission of the pump beam. The blue solid dots with error bars are experimental data and the black solid line is theoretical fit, respectively.

small, the dominant effect on the linewidth is the relaxation Γ_{21} . However, as the Rabi frequency continues to increase, the second (Ω^2) and third (Ω^4) terms in Eq. (14) gradually take effect, thereby increasing the linewidth. Whether it is the influence of optical power or Rabi frequency Ω on linewidth broadening, both belong to power broadening.

C. Fitting and analysis of magnetic resonance spectra excited by cascade two-photon process

The method of analyzing the magnetic resonance signal excited by the cascade two-photon process is the same as that of the magnetic resonance signal excited by Raman

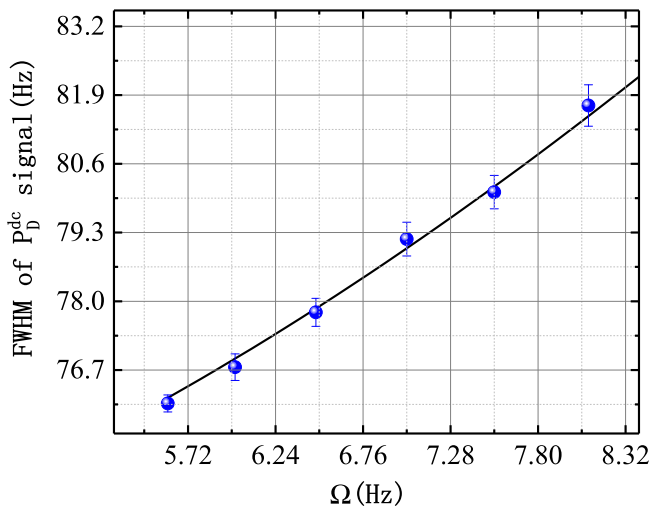


FIG. 9. The full width at half maximum (FWHM) of magnetic resonance transmission spectra of Raman two-photon process for different Ω . The blue solid dots with error bars are experimental data and the black solid line is a theoretical fit.

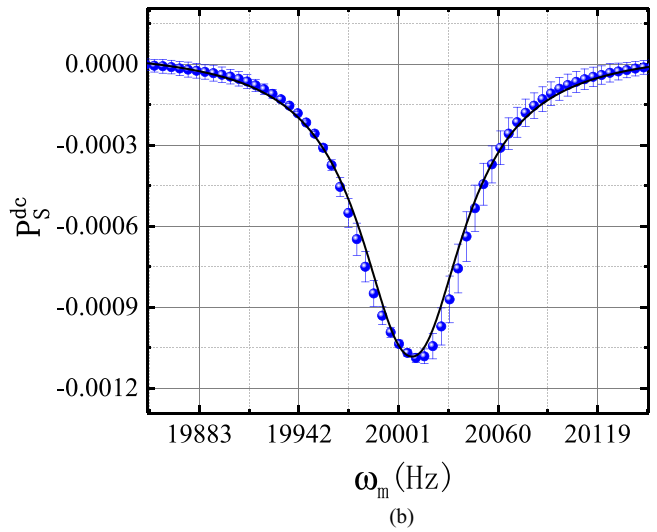
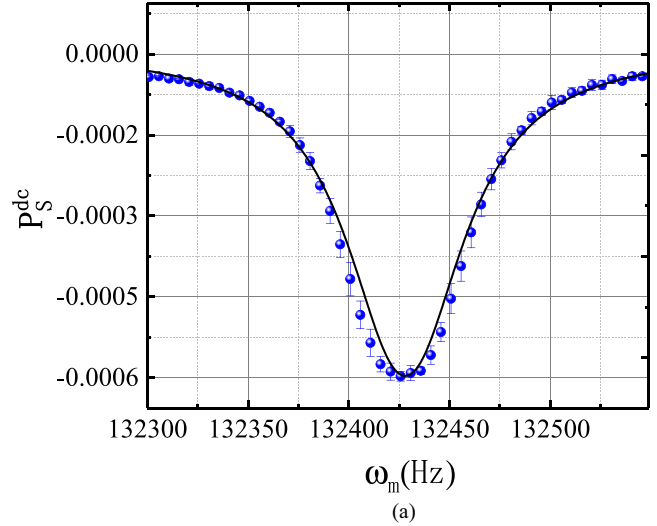


FIG. 10. Resonance spectra of cascade two-photon process, which are plotted as fractional transmission of the pump beam. The solid line (black) is the lineshape of the theoretical analytical solution fitting given by Eqs. (13) with three differently independent relaxation coefficients $\gamma \approx 20$ Hz, $\gamma_{se} \approx 20$ Hz, and $\Gamma_L \approx 33$ Hz. The Rabi frequency Ω_{RF} of the transverse radio-frequency magnetic field is about 1.2 kHz. The blue solid dots with error bars represent the measured experimental data. The optical power is about $10 \mu W$. (a) The frequency ω_m of longitudinal radio-frequency magnetic field is about 132.429 kHz. The frequency ω_{RF} of transverse radio-frequency magnetic field is about 20 kHz. (b) The frequency ω_m of longitudinal radio-frequency magnetic field is about 20.01 kHz. The frequency ω_{RF} of the transverse radio-frequency magnetic field is 132.426 kHz.

two-photon process. It is still satisfying the conditions of the weak pump-probe laser, so as to ensure that all the approximate conditions we do are valid. The experimental measurement results are basically consistent with the theoretical prediction results as shown in Fig. 10(a). By scanning the longitudinal radio-frequency magnetic field \mathbf{B}_m , the center frequencies of magnetic resonance curve are 132.429 kHz. The frequency of the transverse radio-frequency magnetic field \mathbf{B}_{RF} is 20 kHz, and the frequency of the longitudinal

radio-frequency magnetic field \mathbf{B}_m is 132.429 kHz, which always keeps the two radio-frequency magnetic fields and the atom away from resonance conditions. The AC Zeeman shift is about 3 Hz. In Fig. 10(b), the frequency of the transverse radio-frequency magnetic field is 132.426 kHz, and the frequency of the longitudinal radio-frequency magnetic field is about 20.01 kHz. The AC Zeeman shift generated by the transverse radio-frequency magnetic field is about 10 Hz. All experimental data are fit with the same set of parameters. The optical pump relaxation process $\mathcal{L}_L\rho$, the ground-state spin-exchange collision relaxation process $\mathcal{L}_{se}\rho$, and the transit relaxation process $\mathcal{L}_{\text{transit}}\rho$ are dominant. The relaxation rates of atomic multipole moments are the same as those in the case of Raman two-photon process. During the experiment, when a transverse radio frequency magnetic field is used to excite the magnetic resonance, the center frequency of the magnetic resonance is equal to the Larmor precession frequency $\omega_0 = 152.426$ kHz. However, the equivalent center frequency of the magnetic resonance signal excited with cascade two-photon process is about 152.429 kHz in Fig. 10(a). This shows that not only the magnetic resonance signal excited by Raman two-photon process will cause the energy-level shift, but the magnetic resonance excited by cascade two-photon process will also cause an energy-level shift. The reason is similar to that of Raman two-photon process. Figure 11 shows the magnetic resonance transmission spectrum of the cascade two-photon excitation at different optical powers. Similar to the magnetic resonance transmission spectrum excited by the Raman two-photon process, the linewidth of the magnetic resonance transmission spectrum excited by the cascade two-photon process also exhibits power broadening phenomenon.

Based on the above analysis, we can perform precise measurement of the radio-frequency magnetic field through the magnetic resonance signal excited by two-photon process. Without changing the offset field, the frequency and Rabi frequency of a radio-frequency magnetic field can be tuned to measure another radio frequency magnetic field orthogonal to it. When the frequency of the unknown radio frequency magnetic field is lower than the linear split interval of offset magnetic field, the unknown radio frequency field is measured by the magnetic resonance spectrum excited by cascade two-photon process. When the frequency of the unknown radio frequency magnetic field is greater than the Larmor precession frequency generated by the offset magnetic field, the magnetic resonance spectrum excited by Raman two-photon process is used to measure the unknown radio frequency field. This theory can also be applied to the field of magnetic induction tomography (MIT) [21].

IV. CONCLUSION

We present a general theory of magnetic resonance spectrum excited by two-photon processes generated by two orthogonal radio-frequency magnetic fields. The steady-state solutions of the analytic form of atomic multipole moments are given and a detailed analysis was made. In the experiment, the pump-probe method of the linearly polarized light is used to detect the magnetic resonance spectrum. A detailed analysis is made based on the experimental results. According to theoretical values and experimental data, there is a dif-

ference between the magnetic resonance spectra excited by the two-photon processes and the magnetic resonance spectra excited by only a radio-frequency magnetic field. The center frequency of the magnetic resonance spectra excited by only a transverse radio-frequency magnetic field is the Larmor precession frequency. However, the magnetic resonance signal excited by the two-photon processes will have an energy-level shift. The magnitude of the energy-level shift is related to the Rabi frequency Ω_{RF} , the frequency ω_{RF} of the transverse radio-frequency field \mathbf{B}_{RF} , and the atomic splitting frequency ω_0 but has nothing to do with the longitudinal radio frequency field \mathbf{B}_m , which satisfies the relation $\Delta\omega = \frac{\Omega_{\text{RF}}^2}{8} \left(\frac{1}{\omega_0 - \omega_{\text{RF}}} + \frac{1}{\omega_0 + \omega_{\text{RF}}} \right)$. The equivalent Rabi frequency Ω generated by the two-photon processes and atom coupling satisfies the relation $\Omega = \frac{\Omega_{\text{RF}}\Omega_m}{4\omega_m}$. When the frequency ω_{RF} of the transverse radio frequency field \mathbf{B}_{RF} and the frequency ω_m of the longitudinal radio-frequency field \mathbf{B}_m satisfy the condition $\omega_0 + \Delta\omega = \omega_m - \omega_{\text{RF}}$, the Raman two-photon process induces magnetic resonance. In the case of satisfying $\omega_0 + \Delta\omega = \omega_m + \omega_{\text{RF}}$, the cascade two-photon process induces magnetic resonance. In the case of weak Ω_m , the linewidth and peak value of the magnetic resonance spectrum increase with the increase of Ω_m . Finally, according to the characteristics of the magnetic resonance signal, the laser-detected magnetic resonance induced by radio-frequency two-photon processes may be well suited to measure the high bandwidth radio-frequency magnetic field in space [31] and apply to the domain of the magnetic induction tomography [20,63].

ACKNOWLEDGMENTS

This work is supported by the National Natural Science Foundation of China (Grant No. 11774118) and the Fundamental Research Funds for the Central Universities of MOE (Grants No. CCNU18CXTD01, No. CCNU19GF003, and No. CCNU19GF005).

APPENDIX A: DERIVATION OF THE EFFECTIVE HAMILTONIAN OF THE SYSTEM

The Hamiltonian of the system can be expressed as

$$H_{B_{\text{tot}}} = H_0 + H_{\text{int}}, \quad (\text{A1})$$

with

$$H_0 = \omega_0 F_0, \quad (\text{A2})$$

and

$$H_{\text{int}} = \Omega_m F_0 \cos \omega_m t + \frac{1}{\sqrt{2}} \Omega_{\text{RF}} (F_{-1} e^{i\theta} - F_1 e^{-i\theta}) \cos \omega_{\text{RF}} t, \quad (\text{A3})$$

where H_0 is the hyperfine Zeeman splittings generated by the offset magnetic field \mathbf{B}_0 . H_{int} is the interaction term of two orthogonal radio-frequency magnetic fields \mathbf{B}_m and \mathbf{B}_{RF} with atoms. The frequency ω_m of the radio-frequency magnetic field \mathbf{B}_m and the frequency ω_{RF} of the radio-frequency magnetic field \mathbf{B}_{RF} are far from resonance with the frequency ω_0 . The effective Hamiltonian theory [53] is generally used to deal with the Hamiltonian satisfied large detuning conditions. This

method is consistent with the method of time averaging of the Hamiltonian [64]. Introduce transformation $U = e^{-i \int_0^t dt' H_0}$ to

rotate the Hamiltonian $H_{B_{\text{tot}}}$ of the system to the interaction representation, i.e.,

$$H_I = \Omega_m F_0 \cos \omega_m t + \frac{1}{\sqrt{2}} \Omega_{\text{RF}} F_{-1} e^{i\theta} e^{-i\omega_0 t} \cos \omega_{\text{RF}} t - \frac{1}{\sqrt{2}} \Omega_{\text{RF}} F_1 e^{-i\theta} e^{i\omega_0 t} \cos \omega_{\text{RF}} t. \quad (\text{A4})$$

According to the effective Hamiltonian theory [54]: $H_{\text{eff}} = -iH(t) \int^t dt' H(t')$, the interaction Hamiltonian H_I is perturbed to second-order approximation. Therefore, the detailed form of the effective Hamiltonian is given by

$$\begin{aligned} H_{B_{\text{tot}}}^{\text{eff}} = & \left[\frac{\Omega_{\text{RF}}^2}{8(\omega_0 + \omega_{\text{RF}})} + \frac{\Omega_{\text{RF}}^2}{8(\omega_0 - \omega_{\text{RF}})} \right] (F_{-1} F_1 - F_1 F_{-1}) + \frac{\Omega_m^2}{4\omega_m} F_0 F_0 (e^{-i2\omega_m t} - e^{i2\omega_m t}) \\ & + \left[\frac{\Omega_{\text{RF}}^2}{8(\omega_0 - \omega_{\text{RF}})} + \frac{\Omega_{\text{RF}}^2}{8(\omega_0 + \omega_{\text{RF}})} \right] (F_{-1} F_{-1} e^{i2\theta} e^{-i2\omega_0 t} - F_1 F_1 e^{-i2\theta} e^{i2\omega_0 t}) \\ & + \frac{\Omega_{\text{RF}}^2}{8(\omega_0 + \omega_{\text{RF}})} (F_{-1} F_1 e^{i2\omega_{\text{RF}} t} - F_1 F_{-1} e^{-i2\omega_{\text{RF}} t}) + \frac{\Omega_{\text{RF}}^2}{8(\omega_0 - \omega_{\text{RF}})} (F_{-1} F_1 e^{-i2\omega_{\text{RF}} t} - F_1 F_{-1} e^{i2\omega_{\text{RF}} t}) \\ & + \frac{\Omega_{\text{RF}}^2}{8(\omega_0 + \omega_{\text{RF}})} [F_{-1} F_{-1} e^{i2\theta} e^{-i2(\omega_0 + \omega_{\text{RF}})t} - F_1 F_1 e^{-i2\theta} e^{i2(\omega_0 + \omega_{\text{RF}})t}] \\ & + \frac{\Omega_{\text{RF}}^2}{8(\omega_0 - \omega_{\text{RF}})} [F_{-1} F_{-1} e^{i2\theta} e^{-i2(\omega_0 - \omega_{\text{RF}})t} - F_1 F_1 e^{-i2\theta} e^{i2(\omega_0 - \omega_{\text{RF}})t}] \\ & + \frac{\Omega_m \Omega_{\text{RF}}}{4\sqrt{2}(\omega_0 + \omega_{\text{RF}})} [F_0 F_{-1} e^{i\theta} e^{-i(\omega_0 + \omega_m + \omega_{\text{RF}})t} + F_0 F_1 e^{-i\theta} e^{i(\omega_0 + \omega_m + \omega_{\text{RF}})t}] \\ & + \frac{\Omega_m \Omega_{\text{RF}}}{4\sqrt{2}\omega_m} [F_{-1} F_0 e^{i\theta} e^{-i(\omega_0 + \omega_m + \omega_{\text{RF}})t} + F_1 F_0 e^{-i\theta} e^{i(\omega_0 + \omega_m + \omega_{\text{RF}})t}] \\ & + \frac{\Omega_m \Omega_{\text{RF}}}{4\sqrt{2}(\omega_0 + \omega_{\text{RF}})} [F_0 F_{-1} e^{i\theta} e^{-i(\omega_0 - \omega_m + \omega_{\text{RF}})t} + F_0 F_1 e^{-i\theta} e^{i(\omega_0 - \omega_m + \omega_{\text{RF}})t}] \\ & - \frac{\Omega_m \Omega_{\text{RF}}}{4\sqrt{2}\omega_m} [F_{-1} F_0 e^{i\theta} e^{-i(\omega_0 - \omega_m + \omega_{\text{RF}})t} + F_1 F_0 e^{-i\theta} e^{i(\omega_0 - \omega_m + \omega_{\text{RF}})t}] \\ & + \frac{\Omega_m \Omega_{\text{RF}}}{4\sqrt{2}(\omega_0 - \omega_{\text{RF}})} [F_0 F_{-1} e^{i\theta} e^{-i(\omega_0 - \omega_m - \omega_{\text{RF}})t} + F_0 F_1 e^{-i\theta} e^{i(\omega_0 - \omega_m - \omega_{\text{RF}})t}] \\ & - \frac{\Omega_m \Omega_{\text{RF}}}{4\sqrt{2}\omega_m} [F_{-1} F_0 e^{i\theta} e^{-i(\omega_0 - \omega_m - \omega_{\text{RF}})t} + F_1 F_0 e^{-i\theta} e^{i(\omega_0 - \omega_m - \omega_{\text{RF}})t}] \\ & + \frac{\Omega_m \Omega_{\text{RF}}}{4\sqrt{2}(\omega_0 - \omega_{\text{RF}})} [F_0 F_{-1} e^{i\theta} e^{-i(\omega_0 + \omega_m - \omega_{\text{RF}})t} + F_0 F_1 e^{-i\theta} e^{i(\omega_0 + \omega_m - \omega_{\text{RF}})t}] \\ & + \frac{\Omega_m \Omega_{\text{RF}}}{4\sqrt{2}\omega_m} [F_{-1} F_0 e^{i\theta} e^{-i(\omega_0 + \omega_m - \omega_{\text{RF}})t} + F_1 F_0 e^{-i\theta} e^{i(\omega_0 + \omega_m - \omega_{\text{RF}})t}]. \end{aligned} \quad (\text{A5})$$

The Raman two-photon process and the cascade two-photon process are selected from the effective Hamiltonian $H_{B_{\text{tot}}}^{\text{eff}}$, i.e., select the terms satisfying the relationship $\omega_m - \omega_{\text{RF}} - \omega_0 = \delta_D \approx 0$ and $\omega_m + \omega_{\text{RF}} - \omega_0 = \delta_S \approx 0$, respectively. Covariant spherical components of F satisfy the following commutation relations [55]:

$$[F_\mu, F_\nu] = -\sqrt{2} C_{1\mu\nu}^{1\lambda} F_\lambda, \quad [F^2, F_\mu] = 0, \quad (\text{A6})$$

where $\mu, \nu, \lambda = \pm 1, 0$, and $C_{1\mu\nu}^{1\lambda}$ are Clebsch–Gordan coefficients. Therefore, the Hamiltonian of the Raman two-photon process is

$$\begin{aligned} H_D^{\text{eff}} = & \left[\frac{\Omega_{\text{RF}}^2}{8(\omega_0 - \omega_{\text{RF}})} + \frac{\Omega_{\text{RF}}^2}{8(\omega_0 + \omega_{\text{RF}})} \right] F_0 \\ & + \frac{\Omega_m \Omega_{\text{RF}}}{4\sqrt{2}\omega_m} (F_1 e^{-i\theta} e^{-i\delta_D t} - F_{-1} e^{i\theta} e^{i\delta_D t}). \end{aligned} \quad (\text{A7})$$

Similarly, the Hamiltonian of the cascade two-photon process is

$$\begin{aligned} H_S^{\text{eff}} = & \left[\frac{\Omega_{\text{RF}}^2}{8(\omega_0 - \omega_{\text{RF}})} + \frac{\Omega_{\text{RF}}^2}{8(\omega_0 + \omega_{\text{RF}})} \right] F_0 \\ & + \frac{\Omega_m \Omega_{\text{RF}}}{4\sqrt{2}\omega_m} (F_1 e^{-i\theta} e^{-i\delta_S t} - F_{-1} e^{i\theta} e^{i\delta_S t}). \end{aligned} \quad (\text{A8})$$

APPENDIX B: DERIVATION OF EQS. (8), (10), AND (11)

The relaxation process of the system mainly considers the relaxation process of the depopulation of the laser and the repopulation of spontaneous radiation, the relaxation process of the ground-state atomic spin-exchange collision, and the relaxation process of the atoms leaving the laser beam and other atoms injected into the laser beam. In the laboratory frame, the time-dependent evolution of the relaxation process

can be completely described by the master equation of the density operator as

$$\frac{d\rho}{dt} = -i[H_L, \rho] + \mathcal{L}_{sp}\rho + \mathcal{L}_{spin}\rho + \mathcal{L}_{transit}\rho, \quad (\text{B1})$$

where

$$H_L = \Omega_0^* \Sigma_0 + \Omega_0 \Sigma_0^\dagger, \quad (\text{B2})$$

$$\mathcal{L}_{sp}\rho = \Gamma \left(\frac{2J_e + 1}{2J_g + 1} \right) \sum_{q=-1}^1 D[\Sigma_q] \rho. \quad (\text{B3})$$

Here H_L is the Hamiltonian of the linearly polarized laser interacting with atoms, which the laser resonates with the ground state $F_g = 4$ to the excited state $F_e = 3$. Rabi frequency $\Omega_0 := -(J_g \| d \| J_e) E$ is the Rabi frequency of the interaction between atoms and laser and $\langle J_g \| d \| J_e \rangle$ is the reduced electric-dipole matrix element. The coefficient Γ is the spontaneous emission coefficient of the atom. The operator $\mathcal{L}_{sp}\rho$ represents the spontaneous emission relaxation process. The symbols J_g and J_e are the angular-momentum quantum numbers. The operator $D[\Sigma_q] \rho \equiv \Sigma_q \rho \Sigma_q^\dagger - \frac{1}{2} \Sigma_q^\dagger \Sigma_q \rho - \frac{1}{2} \rho \Sigma_q^\dagger \Sigma_q$ is the Lindblad superoperator, with $q = 0, \pm 1$ for the spherical components. The operator Σ_q is the lowering operator in the hyperfine structure and its specific form is

$$\Sigma_q = \sum_{F_g m_g F_e m_e} (-)^{F_e + J_g + 1 + I} \sqrt{S_{F_g F_e} C_{F_g m_g F_e m_e}^{1q}} |F_g m_g\rangle \langle F_e m_e|, \quad (\text{B4})$$

with

$$S_{F_g F_e} := (2F_e + 1)(2J_g + 1) \begin{Bmatrix} J_g & J_e & 1 \\ F_e & F_g & I \end{Bmatrix}^2. \quad (\text{B5})$$

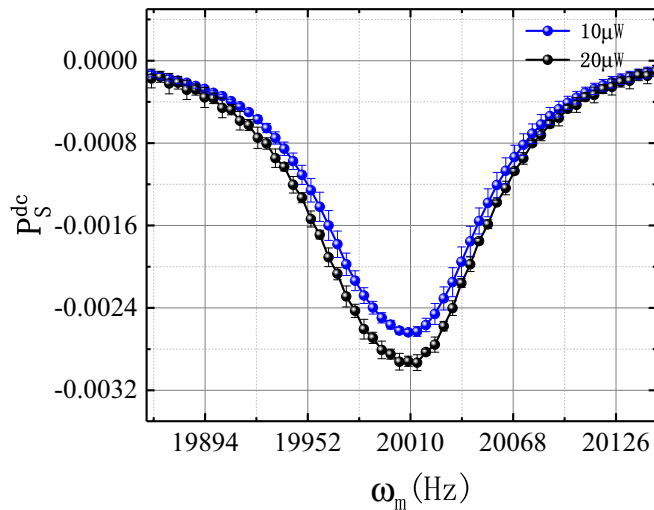


FIG. 11. The magnetic resonance transmission spectra of cascade two-photon process, which is plotted as fractional transmission of the pump beam. The optical powers of blue and black solid dots with error bars are 10 and 20 μW , respectively. The frequency ω_m of longitudinal radio-frequency magnetic field is about 20.009 kHz. The frequency ω_{RF} of the transverse radio-frequency magnetic field is 132.426 kHz.

Here

$$C_{F_g m_g F_e m_e}^{1q} = (-)^{F_e - 1 + m_e} \sqrt{2F_g + 1} \begin{pmatrix} F_e & 1 & F_g \\ m_e & q & -m_g \end{pmatrix},$$

which vanishes unless the sublevels satisfy $m_g = m_e + q$, and $S_{F_g F_e}$ is the hyperfine transition-strength factor [65]. The symbols $(::)$ and $\{\::\}$ are the Wigner 3- j symbol and Wigner 6- j symbol, respectively. Considering that the spontaneous emission relaxation is much greater than the pumping rate of the laser, i.e., $\Gamma \gg \Omega_0$, the excited state is adiabatically eliminated. The master equation enters the ground-state subspace of $F_g = 4$. The depopulation process of laser and the repopulation process of spontaneous radiation are equivalent to three new types of relaxation channels, i.e.,

$$\mathcal{L}_L \rho_g = \Gamma_L \sum_{q=0, \pm 1} D[\Sigma'_q] \rho_g, \quad (\text{B6})$$

with

$$\Sigma'_q = \sum_{m_F} V_{F_e m_F}^{F_g m_F + q} V_{F_g m_F}^{F_e m_F} |F_g m_F + q\rangle \langle F_g m_F|, \quad (\text{B7})$$

where the equivalent relaxation coefficient $\Gamma_L = \frac{64\Omega_0^2}{9\Gamma}$ is the equivalent relaxation coefficient and the operator $D[\Sigma'_q] \rho_g$ is the relaxation Lindblad superoperator. These three types of relaxation channels are σ^- transition type, π transition type, and σ^+ transition type, and the corresponding index q takes $-1, 0, 1$, respectively.

The transition coefficient $V_{F_g m_F}^{F_e m_F}$ is given by

$$V_{F_g m_F}^{F_e m_F} = (-)^{m_F + J + I} \sqrt{(2F + 1)(2F' + 1)(2J + 1)} \times \begin{pmatrix} F' & 1 & F \\ m'_F & q & -m_F \end{pmatrix} \begin{Bmatrix} J & J' & 1 \\ F' & F & I \end{Bmatrix}. \quad (\text{B8})$$

Simultaneously, the relationship of nondiagonal element $\rho_{F_e m_F, F_g m_F}$ between the excited state and the ground state is given by

$$\rho_{F_e m_F, F_g m_F} = \frac{8i V_{F_g m_F}^{F_e m_F} \Omega_0 \rho_{F_g m_F, F_g m_F}}{3\Gamma}, \quad (\text{B9})$$

where such nondiagonal elements are related to detection absorption. Next, we derive the absorption formula of the system. The detection absorption coefficient is given by [58,66]

$$\alpha = \alpha_0 \sum_{m_F} \frac{|V_{F_g m_F}^{F_e m_F} \langle J_g \| d \| J_e \rangle|^2}{V_{F_g m_F}^{F_e m_F} \Omega_0} \text{Im}(\rho_{F_e m_F, F_g m_F}), \quad (\text{B10})$$

where the coefficient $\alpha_0 = 4\pi\omega_0 N / \hbar c$ is just a number. The frequency ω_0 is the transition frequency without magnetic field, N is the atomic density, \hbar is Planck constant, and c is the velocity of light in a vacuum. According to Eqs. (B9) and (B10), the absorption coefficient α is expanded using state multipole as

$$\alpha = \frac{\alpha_0}{9} (14m_{0,0}^{\text{lab}} - \sqrt{77}m_{2,0}^{\text{lab}}), \quad (\text{B11})$$

where the symbols $m_{0,0}^{\text{lab}}$ and $m_{2,0}^{\text{lab}}$ are monopole moment and alignment in the laboratory frame, respectively.

The operator $\mathcal{L}_{spin}\rho$ is the spin-exchange collision relaxation in the ground state of $F_g = 4$. It can be expressed

as $\mathcal{L}_{\text{spin}}\rho = \gamma_{\text{se}}\hat{\rho}_{\text{se}}$, where γ_{se} is the spin-exchange collision relaxation coefficient. The relaxation coefficient $\gamma_{\text{se}} \propto n_{\text{Cs}}$, where n_{Cs} is the cesium-saturated atomic-vapor density [67]. The operator $\hat{\rho}_{\text{se}}$ is the spin-exchange collision relaxation operator [39,68]

$$\hat{\rho}_{\text{se}} = -\frac{3}{4}\rho + \hat{S} \cdot \rho \hat{S} + \langle \hat{S} | \{ \hat{S}, \rho \} - 2i\hat{S} \times \rho \hat{S} \rangle. \quad (\text{B12})$$

Here the symbol $\{.,.\}$ denotes the anticommutator. The third term is the nonlinear effect of collision. In our system, our experimental condition is room temperature, so the particle number density is relatively low. The nonlinear effect caused by spin-exchange collision is not very obvious. Therefore, it is reasonable to ignore the nonlinear term of Eq. (B12). The operator $\hat{S} = (S_x, S_y, S_z)^T$ is the spin operator. The operator $S_{i=x,y,z}$ is defined in the covariant spherical representation as

$$S_x = \frac{1}{\sqrt{2}}(S_{-1} - S_1), \quad (\text{B13a})$$

$$S_y = \frac{i}{\sqrt{2}}(S_{-1} + S_1), \quad (\text{B13b})$$

$$S_z = S_0. \quad (\text{B13c})$$

The notation $|nISFm_F\rangle$ is selected as the basis of the atomic hyperfine structure, where F is the total quantum number, m_F is the quantum number of projection component of F on the quantization axis, S is the electron-spin quantum number, I is the nuclear-spin quantum number and n is the set of the remaining quantum numbers. According to the Wigner-Eckart theorem [57], the matrix elements of the operators $S_{q=0,\pm 1}$ are given by

$$\langle F, m_F | S_q | F', m'_F \rangle = \langle F || S || F' \rangle (-)^{F-m_F} \begin{pmatrix} F' & 1 & F \\ m'_F & q & -m_F \end{pmatrix}, \quad (\text{B14})$$

the reduced density-matrix element $\langle F || S || F' \rangle$ can be further simplified by factoring out the F and F' dependence as

$$\begin{aligned} \langle F || S || F' \rangle &\equiv \langle n, I, S, F || S || n, I, S', F' \rangle \\ &= \langle S || S || S' \rangle (-)^{F'+S+1+I} \sqrt{(2F'+1)(2F+1)} \begin{Bmatrix} S' & F' & I \\ F & S & 1 \end{Bmatrix}, \end{aligned} \quad (\text{B15})$$

where the irreducible density-matrix element $\langle S || S || S' \rangle = \sqrt{3/2}\delta_{SS'}$ in the case of spin an electron. The notation $\delta_{SS'}$ is Kronecker symbol. Therefore, a detailed matrix representation of the operator S_i in the ground state of $F_g = 4$ can be obtained

$$S_x = \frac{1}{\sqrt{2}} \left(\sum_{m_F, m'_F=-4}^4 \langle 4, m_F | S_{-1} | 4, m'_F \rangle | 4, m_F \rangle \langle 4, m'_F | - \sum_{m_F, m'_F=-4}^4 \langle 4, m_F | S_1 | 4, m'_F \rangle | 4, m_F \rangle \langle 4, m'_F | \right), \quad (\text{B16})$$

$$S_y = \frac{i}{\sqrt{2}} \left(\sum_{m_F, m'_F=-4}^4 \langle 4, m_F | S_{-1} | 4, m'_F \rangle | 4, m_F \rangle \langle 4, m'_F | + \sum_{m_F, m'_F=-4}^4 \langle 4, m_F | S_1 | 4, m'_F \rangle | 4, m_F \rangle \langle 4, m'_F | \right), \quad (\text{B17})$$

$$S_z = \sum_{m_F, m'_F=-4}^4 \langle 4, m_F | S_0 | 4, m'_F \rangle | 4, m_F \rangle \langle 4, m'_F |, \quad (\text{B18})$$

where the matrix element $\langle 4, m_F | S_q | 4, m'_F \rangle$ of the spin operator S can be given by Eqs. (B14) and (B15).

The relaxation processes analyzed above are all of the standard Lindblad form. Meanwhile, the relaxation process $\mathcal{L}_{\text{transit}}\rho$ will be processed phenomenologically. The relaxation process $\mathcal{L}_{\text{transit}}\rho$ is given by [57]

$$\mathcal{L}_{\text{transit}}\rho = -\frac{1}{2}\{\kappa, \rho\} + \Lambda. \quad (\text{B19})$$

The first term denotes the relaxation of atoms flying out of the laser beam and the detailed relaxation matrix in the ground state of $F_g = 4$ is then given by

$$\kappa = \gamma \sum_{m_F=-4}^4 | 4, m_F \rangle \langle 4, m_F |, \quad (\text{B20})$$

where the coefficient γ is the transit decay rate. The second term represents the relaxation rate of other atoms flying into the laser beam and the matrix takes the form

$$\Lambda = \frac{\gamma}{9} \sum_{m_F=-4}^4 \rho_{m_F, m_F}^{\text{eq}} | 4, m_F \rangle \langle 4, m_F |, \quad (\text{B21})$$

where the density-matrix element $\rho_{m_F, m_F}^{\text{eq}}$ is the equilibrium population without laser field.

According to the definition of state multipoles

$$m(F'F)_{KQ} = \sum_{M'M} (-)^{F'-M'} \sqrt{2K+1} \begin{pmatrix} F' & F & K \\ M' & -M & Q \end{pmatrix} \langle F'M' | \rho | FM \rangle, \quad (\text{B22})$$

the total relaxation processes are expanded in spherical tensor representation as the relaxation of atomic multipole moment $\mathcal{L}m_{kq}$. According to the Wigner D functions [55], the total relaxation processes of the atomic multipole moments in the laboratory frame xyz is rotated into the rotating frame $x'y'z'$.

Therefore, the time-dependent evolution of the orientation in the frame $x'y'z'$ is given by

$$\dot{m}_{1,0} = -\left(\gamma + \frac{29}{64}\gamma_{se} + \frac{7}{45}\Gamma_L\right)m_{1,0} + i\sqrt{\frac{1}{2}}\Omega e^{-i\theta}m_{1,-1} + i\sqrt{\frac{1}{2}}\Omega e^{i\theta}m_{1,1} + \frac{1}{20}\sqrt{\frac{11}{6}}\Gamma_L m_{3,0}, \quad (\text{B23a})$$

$$\dot{m}_{1,\pm 1} = \left[\mp i\Delta_j - \left(\gamma + \frac{29}{64}\gamma_{se} + \frac{7}{360}\Gamma_L\right)\right]m_{1,\pm 1} + i\sqrt{\frac{1}{2}}\Omega e^{\mp i\theta}m_{1,0} + \frac{1}{60}\sqrt{11}\Gamma_L m_{3,\pm 1}. \quad (\text{B23b})$$

The time-dependent evolution of the alignment in the frame $x'y'z'$ is

$$\dot{m}_{2,0} = -\left(\gamma + \frac{31}{64}\gamma_{se} + \frac{271}{1134}\Gamma_L\right)m_{2,0} + i\sqrt{\frac{3}{2}}\Omega e^{-i\theta}m_{2,-1} + i\sqrt{\frac{3}{2}}\Omega e^{i\theta}m_{2,1} + \frac{19}{378}\sqrt{\frac{13}{2}}\Gamma_L m_{4,0} - \frac{7}{324}\sqrt{77}\Gamma_L m_{0,0}, \quad (\text{B24a})$$

$$\dot{m}_{2,\pm 1} = \left[\mp i\Delta_j - \left(\gamma + \frac{31}{64}\gamma_{se} + \frac{323}{1512}\Gamma_L\right)\right]m_{2,\pm 1} + i\sqrt{\frac{3}{2}}\Omega e^{\mp i\theta}m_{2,0} + i\Omega e^{\pm i\theta}m_{2,\pm 2} + \frac{19}{756}\sqrt{\frac{65}{3}}\Gamma_L m_{4,\pm 1}, \quad (\text{B24b})$$

$$\dot{m}_{2,\pm 2} = \left[\mp i2\Delta_j - \left(\gamma + \frac{31}{64}\gamma_{se} + \frac{26}{189}\Gamma_L\right)\right]m_{2,\pm 2} + i\Omega e^{\mp i\theta}m_{2,\pm 1} + \frac{19}{756}\sqrt{\frac{65}{6}}\Gamma_L m_{4,\pm 2}. \quad (\text{B24c})$$

The time-dependent evolution of hexadecapole moment in the frame $x'y'z'$ is

$$\dot{m}_{4,0} = -\left(\gamma + \frac{19}{32}\gamma_{se} + \frac{380}{693}\Gamma_L\right)m_{4,0} + i\sqrt{5}\Omega e^{-i\theta}m_{4,-1} + i\sqrt{5}\Omega e^{i\theta}m_{4,1} + \frac{35}{198}\sqrt{\frac{35}{26}}\Gamma_L m_{6,0} - \frac{5}{63}\sqrt{\frac{13}{2}}\Gamma_L m_{2,0}, \quad (\text{B25a})$$

$$\begin{aligned} \dot{m}_{4,\pm 1} = & \left[\mp i\Delta_j - \left(\gamma + \frac{19}{32}\gamma_{se} + \frac{1523}{2772}\Gamma_L\right)\right]m_{4,\pm 1} + i\sqrt{5}\Omega e^{\mp i\theta}m_{4,0} + i\sqrt{\frac{9}{2}}\Omega e^{\pm i\theta}m_{4,\pm 2} \\ & + \frac{245}{198}\sqrt{\frac{1}{39}}\Gamma_L m_{6,\pm 1} - \frac{5}{126}\sqrt{\frac{65}{3}}\Gamma_L m_{2,\pm 1}, \end{aligned} \quad (\text{B25b})$$

$$\begin{aligned} \dot{m}_{4,\pm 2} = & \left[\mp i2\Delta_j - \left(\gamma + \frac{19}{32}\gamma_{se} + \frac{383}{693}\Gamma_L\right)\right]m_{4,\pm 2} + i\sqrt{\frac{9}{2}}\Omega e^{\mp i\theta}m_{4,\pm 1} + i\sqrt{\frac{7}{2}}\Omega e^{\pm i\theta}m_{4,\pm 3} \\ & + \frac{49}{99}\sqrt{\frac{5}{39}}\Gamma_L m_{6,\pm 2} - \frac{5}{126}\sqrt{\frac{65}{6}}\Gamma_L m_{2,\pm 2}, \end{aligned} \quad (\text{B25c})$$

$$\dot{m}_{4,\pm 3} = \left[\mp i3\Delta_j - \left(\gamma + \frac{19}{32}\gamma_{se} + \frac{221}{396}\Gamma_L\right)\right]m_{4,\pm 3} + i\sqrt{\frac{7}{2}}\Omega e^{\mp i\theta}m_{4,\pm 2} + i\sqrt{2}\Omega e^{\pm i\theta}m_{4,\pm 4} + \frac{7}{33}\sqrt{\frac{35}{78}}\Gamma_L m_{6,\pm 3}, \quad (\text{B25d})$$

$$\dot{m}_{4,\pm 4} = \left[\mp i4\Delta_j - \left(\gamma + \frac{19}{32}\gamma_{se} + \frac{56}{99}\Gamma_L\right)\right]m_{4,\pm 4} + i\sqrt{2}\Omega e^{\mp i\theta}m_{4,\pm 3} + \frac{35}{198}\sqrt{\frac{7}{26}}\Gamma_L m_{6,\pm 4}. \quad (\text{B25e})$$

According to the Eqs. (B23a)–(B25e), the equivalent radio-frequency magnetic field, the relaxation processes $\mathcal{L}_{\text{transit}}\rho$ and $\mathcal{L}_{se}\rho$ couple together different components of the same order of the atomic multipole moment $m_{k,q}$. However, the linearly polarized light pump relaxation $\mathcal{L}_L\rho_g$ will either couple the even-order atomic multipole moments $m_{k,q}$ together, or couple the odd-order atomic multipole moments together. The steady-state equations of even-order atomic multipole moments are linear inhomogeneous equations. Therefore, the physical evolution of the system is determined by the even-order atomic multipole moments. Considering the weak pumping condition, the hexadecapole moments and higher-order multipole moments can be omitted. Therefore, it is reasonable to simulate the evolution of the system by calculating the evolution of the alignment.

At the same time, according to Eq. (B11), the DC component of the absorption coefficient in the frame $x'y'z'$ is

$$\alpha = \frac{\alpha_0}{9} \left(14m_{0,0} + \frac{\sqrt{77}}{2}m_{2,0} \right). \quad (\text{B26})$$

APPENDIX C: VISUALIZATION OF STEADY-STATE ATOMIC POLARIZATION OF THE SYSTEM

The visualization of the steady-state atomic polarization of the system is given by the angular-momentum probability surfaces which is extremely useful for studying and understanding the symmetry of higher-order multipole moments and atomic polarization of atomic ensemble. The probability of finding the maximum value of the angular-momentum pro-

jection in the polar angles β and φ is given by [57,69]

$$r(\beta, \varphi) = \langle m = F | \rho(\beta, \varphi) | m = F \rangle \quad (\text{C1})$$

with

$$\rho(\beta, \varphi) = R^{-1}(\varphi, \theta, 0) \rho R(\varphi, \beta, 0), \quad (\text{C2})$$

where $R(\varphi, \beta, \gamma)$ is the rotation matrix and ρ is the density matrix. According to Eqs. (B23a)–(B25e), the steady-state evolution of the system is mainly contributed by the even-order atomic multipole moments. Further considering, it is reasonable to simplify the system to alignment system under the condition of satisfying the weak light pumping. In the laboratory frame xyz , the expression of the angular-momentum probability surface of our system can be analytically given by

$$\begin{aligned} r(\beta, \varphi, t) &= \sqrt{\frac{4\pi}{9}} m_{0,0}^{\text{lab}}(t) Y_{0,0}(\beta, \varphi) \\ &+ \sqrt{\frac{4\pi}{9}} \sqrt{\frac{28}{55}} \sum_{q=-2}^2 m_{2,q}^{\text{lab}}(t) Y_{2,q}(\beta, \varphi) \\ &= \sqrt{\frac{4\pi}{9}} D_{00}^0\left(\frac{\pi}{2}, \frac{\pi}{2}, \pi\right) m_{0,0}(t) Y_{0,0}(\beta, \varphi) \quad (\text{C3}) \\ &+ \sqrt{\frac{4\pi}{9}} \sqrt{\frac{28}{55}} \sum_{q', q=-2}^2 m_{2,q'}(t) \\ &\times D_{q'q}^{2*}\left(\frac{\pi}{2}, \frac{\pi}{2}, \pi\right) Y_{2,q}(\beta, \varphi), \end{aligned}$$

where $m_{k,q}^{\text{lab}}(t)$ and $m_{k,q}(t)$ are the state multipoles of the atomic ensemble in the laboratory frame xyz and in the rotating frame $x'y'z'$, respectively. The special function $Y_{lm}(\beta, \varphi)$ is the spherical harmonics with the polar axis z in the laboratory frame xyz . The symbol $D_{q'q}^k(\phi, \vartheta, \psi)$ is the Wigner D functions with the arguments ϕ, ϑ, ψ , and the indicators q' and q are in the range from $-k$ to k . When $t \rightarrow \infty$, i.e., the atomic ensemble reaches its steady state, and the atomic alignment can be given by

$$m_{2,q}(t) = m_{2,q}(\infty) e^{-iq(\omega_m \pm \omega_{\text{RF}})t}. \quad (\text{C4})$$

Here $m_{2,q}(\infty)$ is the steady-state solution of Eq. (8). The subscript q takes 0, ± 1 , and ± 2 corresponding to the DC component of the alignment, the first-harmonic component of the alignment and the second-harmonic component of the alignment [43], respectively. During the experiment, the scanning time of the radio-frequency magnetic field is 5 s and the relaxation time of the atom is about 0.025 s (the half-width at half maximum of atoms is about 40 Hz), so the system is in a steady state throughout the scanning process. The terms containing the first harmonic signal $m_{2,\pm 1}(\infty) e^{\mp i(\omega_m \pm \omega_{\text{RF}})t}$ and the second-harmonic signal $m_{2,\pm 2}(\infty) e^{\mp 2i(\omega_m \pm \omega_{\text{RF}})t}$ are fast oscillating terms, and the time period average values are 0. Therefore, under the condition of $t \rightarrow \infty$ ($t \gg 1/\Gamma_{2q}$), i.e., the system is in a steady state, only the DC terms $m_{0,0}(\infty)$ and $m_{2,0}(\infty)$ affect the polarized form of atomic ensemble. Simultaneously, the transmission spectrum detected by the pump-probe light field is also the steady-state DC components $m_{0,0}(\infty)$ and $m_{2,0}(\infty)$. To clearly describe the physical picture

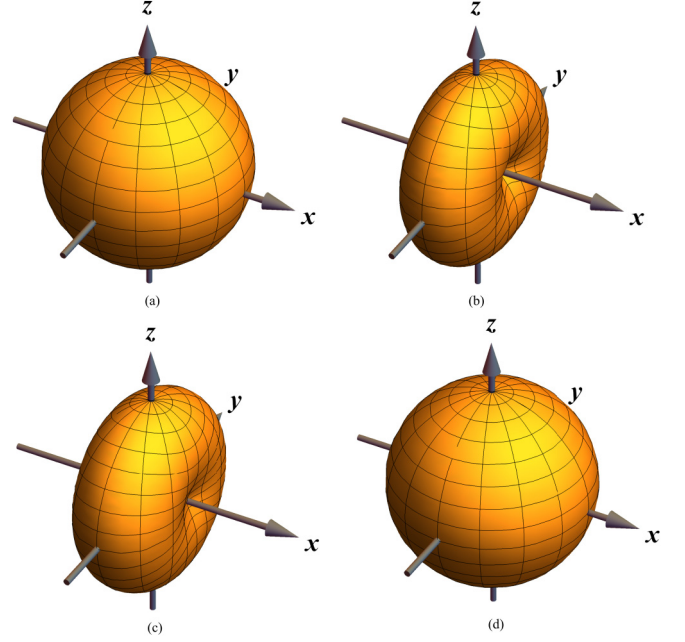


FIG. 12. In the laboratory frame xyz where the quantum axis is along the direction of light polarization, the atomic ensemble exhibits different polarization states with removing any contribution of the rotating terms $m_{2,q}(q \neq 0)$. (a) The atomic ensemble without any relaxation processes and the equivalent radio-frequency excitation produced by the cascade two-photon process. (b) The steady-state polarization of atomic ensemble in the absence of the equivalent radio-frequency excitation produced by the cascade two-photon process. (c) The steady-state polarization of atomic ensemble in the presence of the equivalent resonant radio-frequency excitation produced by the cascade two-photon process in the x direction. (d) The atomic ensemble with the spin-exchange collision relaxation process $\mathcal{L}_{se}\rho$, transit relaxation process $\mathcal{L}_{\text{transit}}\rho$ and the equivalent resonant radio-frequency excitation produced by the cascade two-photon process in the absence of optical-pump relaxation process $\mathcal{L}_L\rho_g$.

explained by the angular-momentum probability surfaces, the simplified analytical expression is transparently given by

$$\begin{aligned} r(\infty) &= \sqrt{\frac{4\pi}{9}} m_{0,0}(\infty) Y_{0,0}(\beta, \varphi) \\ &- \sqrt{\frac{4\pi}{9}} \sqrt{\frac{28}{55}} \frac{1}{2} m_{2,0}(\infty) Y_{2,0}(\beta, \varphi) \\ &+ \sqrt{\frac{4\pi}{9}} \sqrt{\frac{28}{55}} \frac{\sqrt{6}}{4} m_{2,0}(\infty) [Y_{2,2}(\beta, \varphi) + Y_{2,-2}(\beta, \varphi)] \\ &= \sqrt{\frac{4\pi}{9}} m_{0,0}(\infty) Y_{0,0}(\beta', \varphi') \\ &+ \sqrt{\frac{4\pi}{9}} \sqrt{\frac{28}{55}} m_{2,0}(\infty) Y_{2,0}(\beta', \varphi'), \quad (\text{C5}) \end{aligned}$$

where $Y_{k,q}(\beta', \varphi')$ is the spherical harmonic function with the polar axis z' in the rotating frame $x'y'z'$. Figure 12 shows the angular-momentum probability surfaces of the atomic ensemble in the steady state. Through the phenomena described in the Fig. 12(b), the optical pump relaxation process $\mathcal{L}_L\rho_g$ polarizes atoms symmetrically along the quantization axis

x in the laboratory frame xyz , which coincides with the z' axis in the rotating frame $x'y'z'$. This is consistent with the physical picture expressed by Eq. (C5). Figure 12(c) shows the equivalent radio-frequency excitation by the cascade two-photon process will destroy the atomic polarization. The equivalent radio-frequency excitation produced by the Raman

two-photon and the equivalent radio-frequency excitation produced by the cascade two photon have the same effect on the polarization of the atomic ensemble. Since the spin-exchange relaxation and transit relaxation processes are isotropic, these two losses do not contribute to the polarization of the atomic ensemble.

-
- [1] W. Denk, J. H. Strickler, and W. W. Webb, *Science* **248**, 73 (1990).
- [2] P. Dufour, M. Piché, Y. D. Koninck, and N. McCarthy, *Appl. Opt.* **45**, 9246 (2006).
- [3] D. A. Parthenopoulos and P. M. Rentzepis, *Science* **245**, 843 (1989).
- [4] B. H. Cumpston, S. P. Ananthavel, S. Barlow, D. L. Dyer, J. E. Ehrlich, L. L. Erskine, A. A. Heikal, S. M. Kuebler, I.-Y. Sandy Lee, D. McCord-Maughon *et al.*, *Nature (London)* **398**, 51 (1999).
- [5] K. Svoboda and R. Yasuda, *Neuron* **50**, 823 (2006).
- [6] S. Maruo, O. Nakamura, and S. Kawata, *Opt. Lett.* **22**, 132 (1997).
- [7] W. L. Peticolas, J. P. Goldsborough, and K. E. Rieckhoff, *Phys. Rev. Lett.* **10**, 43 (1963).
- [8] H. K. Avetissian, A. K. Avetissian, B. R. Avchyan, and G. F. Mkrtchian, *Phys. Rev. B* **100**, 035434 (2019).
- [9] Y.-X. Liu, J. Q. You, L. F. Wei, C. P. Sun, and F. Nori, *Phys. Rev. Lett.* **95**, 087001 (2005).
- [10] F. Deppe, M. Mariani, E. P. Menzel, A. Marx, S. Saito, K. Kakuyanagi, H. Tanaka, T. Meno, K. Semba, H. Takayanagi, E. Solano, and R. Gross, *Nat. Phys.* **4**, 686 (2008).
- [11] E. C. Diniz, D. Z. Rossatto, and C. J. Villas-Boas, *Quantum Inf. Process.* **17**, 202 (2018).
- [12] K. Moon and S. M. Girvin, *Phys. Rev. Lett.* **95**, 140504 (2005).
- [13] Cohen-Tannoudji, *C. R. Phys.* **20**, 658 (2019).
- [14] D. Nettels, R. Müller-Siebert, S. Ulzega, and A. Weis, *Appl. Phys. B: Lasers Opt.* **77**, 563 (2003).
- [15] G. S. Agarwal, T. N. Dey, and D. J. Gauthier, *Phys. Rev. A* **74**, 043805 (2006).
- [16] F. Beato, E. Belorizky, E. Labyt, M. Le Prado, and A. Palacios-Laloy, *Phys. Rev. A* **98**, 053431 (2018).
- [17] G. Bevilacqua, V. Biancalana, A. Vigilante, T. Zanon-Willette, and E. Arimondo, *Phys. Rev. Lett.* **125**, 093203 (2020).
- [18] D. Budker, D. F. Kimball, and D. P. DeMille, *Atomic Physics* (Oxford University Press, New York, 2008).
- [19] C. Deans, L. Marmugi, S. Hussain, and F. Renzoni, *Appl. Phys. Lett.* **108**, 103503 (2016).
- [20] P. Bevington, R. Gartman, and W. Chalupczak, *J. Appl. Phys.* **125**, 094503 (2019).
- [21] A. Wickenbrock, N. Leefer, J. W. Blanchard, and D. Budker, *Appl. Phys. Lett.* **108**, 183507 (2016).
- [22] P. Bevington, R. Gartman, and W. Chalupczak, *Rev. Sci. Instrum.* **90**, 013103 (2019).
- [23] H. Xia, A. Ben-Amar Baranga, D. Hoffman, and M. V. Romalis, *Appl. Phys. Lett.* **89**, 211104 (2006).
- [24] I. Altarev, Y. Borisov, N. Borovikova, A. Egorov, S. Ivanov, E. Kolomensky, M. Lasakov, V. Nazarenko, A. Pirozhkov, A. Serebrov, Y. Sobolev, E. Shulgina, and V. Lobashev, *Phys. Atom. Nucl.* **59**, 1152 (1996).
- [25] P. Bevington, R. Gartman, and W. Chalupczak, *Appl. Phys. Lett.* **115**, 173502 (2019).
- [26] V. V. Talanov, N. M. Lettsome, V. Borzenets, N. Gagliolo, A. B. Cawthorne, and A. Orozco, *Supercond. Sci. Technol.* **27**, 044032 (2014).
- [27] R. C. Black, F. C. Wellstood, E. Dantsker, A. H. Miklich, D. Koelle, F. Ludwig, and J. Clarke, *Appl. Phys. Lett.* **66**, 1267 (1995).
- [28] D. Budker and M. Romalis, *Nat. Phys.* **3**, 227 (2007).
- [29] S. J. Smullin, I. M. Savukov, G. Vasilakis, R. K. Ghosh, and M. V. Romalis, *Phys. Rev. A* **80**, 033420 (2009).
- [30] A. Grosz, M. J. Haji-Sheikh, and S. C. Mukhopadhyay, *High Sensitivity Magnetometers* (Springer International Publishing, Switzerland, 2017).
- [31] I. M. Savukov, S. J. Seltzer, M. V. Romalis, and K. L. Sauer, *Phys. Rev. Lett.* **95**, 063004 (2005).
- [32] N. Castagna and A. Weis, *Phys. Rev. A* **84**, 053421 (2011).
- [33] P.-L. Qi, X.-X. Geng, G.-Q. Yang, G.-M. Huang, and G.-X. Li, *J. Opt. Soc. Am. B* **37**, 3303 (2020).
- [34] C. Cohen-Tannoudji and A. Kastler, *Progress in Optics* **5**, 1 (1966).
- [35] W. Happer, *Rev. Mod. Phys.* **44**(2), 169 (1972).
- [36] D. Sheng, S. Li, N. Dural, and M. V. Romalis, *Phys. Rev. Lett.* **110**, 160802 (2013).
- [37] R. Li, W. Fan, L. Jiang, L. Duan, W. Quan, and J. Fang, *Phys. Rev. A* **94**, 032109 (2016).
- [38] Y. Shi and A. Weis, *Eur. Phys. J. D* **72**, 73 (2018).
- [39] T. Scholtes, S. Pustelny, S. Fritzsche, V. Schultze, R. Stolz, and H.-G. Meyer, *Phys. Rev. A* **94**, 013403 (2016).
- [40] S. J. Ingleby, C. O'Dwyer, P. F. Griffin, A. S. Arnold, and E. Riis, *Phys. Rev. A* **96**, 013429 (2017).
- [41] G. Q. Yang, H.-B. Zhang, X.-X. Geng, S.-Q. Liang, Y. F. Zhu, J.-T. Mao, G.-M. Huang, and G.-X. Li, *Opt. Express* **26**, 30313 (2018).
- [42] Y. Chang, Y.-H. Guo, and J. Qin, *Phys. Rev. A* **99**, 063411 (2019).
- [43] A. Weis, G. Bison, and A. S. Pazgalev, *Phys. Rev. A* **74**, 033401 (2006).
- [44] E. Breschi and A. Weis, *Phys. Rev. A* **86**, 053427 (2012).
- [45] S. J. Ingleby, C. O'Dwyer, P. F. Griffin, A. S. Arnold, and E. Riis, *Phys. Rev. Appl.* **10**, 034035 (2018).
- [46] B. Cai, C.-P. Hao, Z.-R. Qiu, Q.-Q. Yu, W. Xiao, and D. Sheng, *Phys. Rev. A* **101**, 053436 (2020).
- [47] D. Budker, *Nature (London)* **422**, 574 (2003).
- [48] G. Di Domenico, H. Saudan, G. Bison, P. Knowles, and A. Weis, *Phys. Rev. A* **76**, 023407 (2007).
- [49] S. L. Kemp, I. G. Hughes, and S. L. Cornish, *J. Phys. B: At., Mol. Opt. Phys.* **44**, 235004 (2011).
- [50] J. M. Choi, J. M. Kim, and D. Cho, *Phys. Rev. A* **76**, 053802 (2007).

- [51] D. Budker, W. Gawlik, D. F. Kimball, S. M. Rochester, V. V. Yashchuk, and A. Weis, *Rev. Mod. Phys.* **74**, 1153 (2002).
- [52] D. Budker, D. F. Kimball, V. V. Yashchuk, and M. Zolotarev, *Phys. Rev. A* **65**, 055403 (2002).
- [53] W. J. Shao, C. F. Wu, and X.-L. Feng, *Phys. Rev. A* **95**, 032124 (2017).
- [54] R. Tan, G.-X. Li, and Z. Ficek, *Phys. Rev. A* **78**, 023833 (2008).
- [55] D. A. Varshaloich, A. N. Moskalev, and V. K. Khersonskii, *Quantum Theory of Angular Momentum* (World Scientific, Singapore, 1988).
- [56] K. Blum, *Density Matrix Theory and Applications*, 2nd ed. (Plenum Press, New York, 1996).
- [57] M. Auzinsh, D. Budker, and S. M. Rochester, *Optically Polarized Atoms* (Oxford University Press, New York, 2010).
- [58] L. Margalit, M. Rosenbluh, and A. D. Wilson-Gordon, *Phys. Rev. A* **87**, 033808 (2013).
- [59] H.-T. Zhou, D.-W. Wang, D. Wang, J.-X. Zhang, and S.-Y. Zhu, *Phys. Rev. A* **84**, 053835 (2011).
- [60] G. Di Domenico, G. Bison, S. Groeger, P. Knowles, A. S. Pazgalev, M. Rebetez, H. Saudan, and A. Weis, *Phys. Rev. A* **74**, 063415 (2006).
- [61] A. J. Poustie and M. H. Dunn, *Phys. Rev. A* **47**, 1365 (1993).
- [62] G.-X. Li and J.-S. Peng, *Phys. Rev. A* **52**, 465 (1995).
- [63] H. Griffiths, *Meas. Sci. Technol.* **12**, 1126 (2001).
- [64] A. P. Saiko, S. A. Markevich, and R. Fedaruk, *Phys. Rev. A* **98**, 043814 (2018).
- [65] D. A. Steck, *Cesium D Line Data* **4710**, 1 (2008).
- [66] S. Menon and G. S. Agarwal, *Phys. Rev. A* **59**, 740 (1999).
- [67] N. Castagna, G. Bison, G. Di Domenico, A. Hofer, P. Knowles, C. Macchione, H. Saudan, and A. Weis, *Appl. Phys. B: Lasers Opt.* **96**, 763 (2009).
- [68] Y. Shi, T. Scholtes, Z. D. Grujic, V. Lebedev, V. Dolgovskiy, and A. Weis, *Phys. Rev. A* **97**, 013419 (2018).
- [69] S. M. Rochester and D. Budker, *Am. J. Phys.* **69**, 450 (2001).